Science of Remote Sensing 10 (2024) 100160

Contents lists available at ScienceDirect

Science of Remote Sensing

journal homepage: www.sciencedirect.com/journal/science-of-remote-sensing

Characterizing forest structural changes in response to non-stand replacing disturbances using bitemporal airborne laser scanning data

Tommaso Trotto [a,*], Nicholas C. Coops [a], Alexis Achim [b], Sarah E. Gergel [c], Dominik Roeser [a]

[a] Department of Forest Resources Management, University of British Columbia, 2424 Main Mall, Vancouver, BC, V6T 1Z4, Canada

[b] Centre de recherche sur les matériaux renouvelables, Département des sciences du bois et de la forêt, Université Laval, 2425 rue de la Terrasse, Québec, QC, G1V 0A6, Canada

[c] Department of Forest and Conservation Sciences, Faculty of Forestry, University of British Columbia, 2424 Main Mall, Vancouver, BC, V6T 1Z4, Canada

ARTICLE INFO

Keywords:
Boreal forest
Insect
Lidar
Disturbance severity
Canopy cover
Clustering

ABSTRACT

Characterizing the extent, severity, and persistence of natural disturbances in forests is crucial in areas as large and heterogeneous as the Canadian boreal forest. Non-stand replacing (NSR) disturbances, in particular, can produce subtle and lagged impacts to forest canopy and structure with mechanisms that remain elusive, and they are challenging to discern using typical remote sensing approaches including aerial photointerpretation and spectral analysis of satellite imagery. Consequently, there is a need for timely and accurate information on the structural modifications due to NSR disturbances to inform proactive forest management practices. To address these needs, we leveraged a unique bitemporal airborne laser scanning (ALS) dataset to characterize changes in the forest structure caused by eastern spruce budworm (ESB, *Choristoneura fumiferana* (Clem.)), responsible for one of the greatest tree mortality in Canada. A range of infestation severity with varying impacts to forest structure are examined in a mixedwood boreal forest in Lac-Saint Jean, Quebec, Canada. We derived 14 ALS structural change metrics at 10 m spatial resolution, including height, cover, and gappiness 7 years apart (2014–2020). Six distinct structural responses to cumulative ESB infestations severity were identified using cluster analysis from the combination of the 14 change metrics, with canopy cover, the 75th and 25th height percentiles (p75-25) driving cluster separability. Canopy cover and p25 consistently decreased as cumulative infestation severity increased, whereas p75 showed greater variability across the landscape. Photointerpretation of aerial imagery over the same period confirmed the validity of the structural characterization. Further, we studied the role of initial forest structures in modulating the severity of the infestation and found that sparser canopies with cover <65% and shorter trees (p75 < 7.5 m, p25 < 2.5 m) were associated with less severe ESB infestations after 7 years, and controlling for underlying environmental factors. These findings showed the potential of bitemporal ALS data in characterizing structural changes due to ESB infestations at fine scale based on canopy cover and height, relevant for forest management strategies to better target current and future infestations.

1. Introduction

Natural disturbances play a major role in shaping forest dynamics, including species successional pathways and shifting dominance (Cohen et al., 2016), nutrient cycling and tree growth (Maynard et al., 2014), and forest structural complexity development (Turner, 2010). These disturbances exhibit idiosyncratic regimes defined by frequency, size, severity, and are sensitive to climate change (Seidl et al., 2017). As a result, disturbances such as wildfires, insect outbreaks, and windthrows manifest across varying spatial and temporal scales, affecting entire stands, tree patches, or individual trees. Stand-replacing (SR) disturbances are characterized by large and abrupt modifications in the forest structure (Turner, 2010). Conversely, small-to-moderate severity non-stand replacing (NSR) disturbances exhibit more complex and additive ecological responses on the forest structure (Buma, 2015; Kleinman et al., 2019; Piggott et al., 2015; Turner, 2010). Forest structure is the forest's physical geography, that is the 3-dimensional (3D) distribution and arrangement of trees and other plants over a range of spatial scales, and includes characteristics like vertical species stratification, canopy continuity and geometry, species patchiness, and age

* Corresponding author.
E-mail address: tommaso.trotto@ubc.ca (T. Trotto).

https://doi.org/10.1016/j.srs.2024.100160
Received 23 April 2024; Received in revised form 28 August 2024; Accepted 30 August 2024
Available online 31 August 2024
2666-0172/© 2024 The Authors. Published by Elsevier B.V. This is an open access article under the CC BY-NC-ND license (http://creativecommons.org/licenses/by-nc-nd/4.0/).

distribution (Seidler and Bawa, 2001).

NSR disturbances including surface fires, insect defoliations, localized windthrows, and droughts may render subtle yet widespread tree mortality that is often challenging to observe due to incomplete and protracted losses in canopy structural properties across varying spatial and temporal scales (Peng et al., 2011). NSR disturbances may reorganize tree spatial arrangements by creating canopy gaps (Hart and Kleinman, 2018), alter within-canopy complexity and tree height, and result in mixed responses on tree growth (Atkins et al., 2020; Coops et al., 2020) depending on the specific disturbance agent involved. One such example is eastern spruce budworm (ESB – *Choristoneura fumiferana (Clem.)),* a native defoliator in eastern North America. It naturally inhabits all spruce and fir forests, with balsam fir (*Abies balsamea* L. (Mill)) being particularly vulnerable as primary host species. As infestations become more severe, attacks extend to secondary host species including white spruce (*Picea glauca,* (Moench) Voss) and black spruce (*Picea mariana* Mill.) (Bognounou et al., 2017; Nealis and Régnière, 2004).

Repeated ESB attacks lead to changes in the forest structure and composition, as well as understory recruitment by favoring a mixture of host and non-host species (e.g. *Betula* spp.), similarly to gap dynamics (Bouchard et al., 2006a, 2006b; Bouchard and Pothier, 2010; Kneeshaw et al., 2022). These patterns are influenced by geographic gradients, stand characteristics such as species mixtures (Bouchard and Pothier, 2010), initial stand conditions (Choi et al., 2023), and climate factors (Gray, 2008; MacLean, 1984). ESB infestations can reduce canopy cover (Bouchard et al., 2006a), impact tree height (Goodbody et al., 2018), result in incomplete loss of foliage (Virgin and MacLean, 2017), and present varying degree of spatial aggregation depending on the severity of the infestation, with more severe infestations showing a more clumped organizations within a matrix of lighter infestations (Bouchard and Pothier, 2010). Moreover, the transition from endemic to epidemic population density has been attributed to complex within and between population dynamics; however, the persistence of endemic populations has highlighted the susceptibility of any spruce-fir forest to ESB population escalation to an epidemic level (Mattson et al., 1988). Consequently, currently undisturbed areas simply have not yet developed environmental and biological conditions favorable for ESB population growth to reach epidemic levels (Mattson et al., 1988).

Traditionally, our understanding of ESB infestations come from dendrochronological data and aerial surveys which are periodically interpreted, along with field records to validate the accuracy of the interpretation (Goodbody et al., 2018). Photointerpretation results in the delineation of defoliation classes including severe, intermediate, and light (Goodbody et al., 2018; Ministère des Ressources naturelles et des Forêts, 2023a). However, the distribution and size of the attacks may be approximate, the interpretation of the aerial photos may potentially provide limited temporal and spatial information on disturbance distribution (Lepš and Hadincová, 1992; Lunetta et al., 1991; Thompson et al., 2007), and they are more inclined to capture larger scale disturbances across broad areas. These limitations make detection and characterization or light and intermediate attacks challenging, especially at fine scale (Coops et al., 2020).

There has been growing attention to the use of multi-source remote sensing tools for insect disturbance characterization at broad and fine scales (Achim et al., 2022; Coops et al., 2023; Senf et al., 2017; Trumbore et al., 2015). In particular, the widespread adoption of lidar technologies such aerial laser scanning systems (ALS) has expanded the availability of 3D data capturing the spatial and temporal distribution of forest structural attributes (i.e. point cloud), with higher accuracies compared to traditional approaches based on field measurements. The increasing availability of bitemporal and multitemporal ALS point clouds allows for wall-to-wall, fine-scale structural change characterization by leveraging small acquisition footprints and high number of returns for discrete sensors, thereby offering additional insights into structural alterations resulting from insect attacks of varying severity. For instance, Choi et al. (2023) investigated the impact of insect attacks, along with other NSR disturbances such as diseases small wildfires, on changes in the forest structure using multitemporal ALS data. Their results revealed that structural responses were contingent upon the specific disturbance agent, time since disturbance, initial canopy complexity, and the structural attribute under analysis derived from ALS (hereafter ALS metrics). Tompalski et al. (2021) synthesized numerous studies that adopted multitemporal ALS datasets for change detection in forestry, demonstrating the feasibility of ALS in characterizing changes in forest attributes at varying spatial and temporal scales under different forest types.

However, few studies have examined changes in forest structural attributes as derived from ALS due to ESB infestations in a sensitive ecosystem such as the eastern Canadian mixed boreal forest. Repeated ALS acquisitions in these regions are rare and present challenges. As a result of rapid technological advancements, ALS sensors are designed with differing specifications in terms of point density, pulse frequency, scanning angle, type (e.g. single photon lidar), and varying vertical and horizontal accuracy (White et al., 2016). Consequently, data harmonization across acquisitions may be necessary to minimize inconsistencies, ensuring that detected change represents true change and not systematic data differences (Lague et al., 2013; Riofrío et al., 2022), for example resulting from georeferencing errors (Zhang and Shen, 2013). Common approaches for data harmonization include pairwise point cloud registration, density thinning, and normalization using the same digital terrain model (DTM). Mathematical frameworks have been proposed to remove bias attributable to variation in point density, footprint size and beam incidence angle (Roussel et al., 2017, 2018) and studies reported statistically significant differences in tree height increment estimates for tree growth modeling purposes between harmonized and non-harmonized data (Riofrío et al., 2022). Following harmonization, change detection and characterization may be performed directly on the point cloud (Kharroubi et al., 2022; Lague et al., 2013; Xu et al., 2015). These approaches are sensitive to variations in intra- and inter-cloud point density and distribution and may be more challenging to apply in a forestry context due to the naturally high variability in the forest structures over time and varying scanning positions along flightlines for airborne lidar systems. Alternatively, raster differencing entails the repeated rasterizations of ALS metrics from point clouds, such as height, canopy cover, or eigen-based metrics describing canopy shape (Lucas et al., 2019), which are subtracted over time. This approach is particularly suitable in a forestry context where inherent differences in point clouds over time are expected, and consists of regularizing 3D point cloud information onto a 2-dimensional (2D) grid. Raster differencing reduces the change detection error associated with systematic and random changes in point distribution over time and simplifies change characterization and interpretation by comparing changes at the pixel level instead of relying on point data (Choi et al., 2023; Marinelli et al., 2018; Vastaranta et al., 2013).

In this study, we focused on the characterization of structural changes resulting from extensive ESB infestations of varying severity given the availability of a bitemporal ALS dataset in the mixed boreal forests of Lac Saint-Jean (LSJ), Quebec, Canada acquired 7 years apart (2014–2020). Since ESB infestations mostly result in foliage changes in the early stages of an attack, which are expected to negatively affect tree growth and biomass by influencing tree height, canopy cover, leaf area, and canopy shape, our characterization of structural changes largely pertained to changes in these biomass-related structural attributes. In particular, our objective was twofold. First, we characterized these structural changes using a raster differencing approach and cluster analysis on a number of ALS metrics suited for describing the subtle impact of insect infestations (Atkins et al., 2020; Bouchard and Pothier, 2010), and we validated the results via photointerpretation. Second, we investigated the role of initial forest structures in modulating the severity of ESB infestations. We described this modulating effect as forest structures typified by lower infestation severity at the end of the analyzed period. To do so, we compared initial structures that resulted in low versus high infestation severity while controlling for local environmental conditions.

2. Study area and data

2.1. Study area description

The study was conducted in Lac Saint-Jean, Quebec, Canada (Fig. 1), a boreal mixedwood forested region extending over approximately 20,355 km^2. It encompasses two bioclimatic domains. The Balsam Fir – Yellow Birch (*Abies balsamea* (L.) Mill. – *Betula alleghaniensis* Britt.) domain and the Spruce – Feathermoss domain. The Balsam Fir – Yellow Birch domain presents a mixed stand composition of balsam fir, yellow birch, Eastern cedar (Thuja occidentalis L.), and white spruce. The Spruce – Feathermoss domain extends to the northernmost part of LSJ, with forest land mostly dominated by balsam fir and black spruce, along with hardwood species such as trembling aspen (*Populus tremuloides* Michx.) and white birch (*Betula papyrifera* Marshall). Forest types cover an area of approximately 11,500 km^2 of conifers, 1800 km^2 of mixedwood species, and 400 km^2 of deciduous according to the provincial forest resource inventory (FRI). LSJ is surrounded by the Laurentian highlands and is located between approximately 60 m and 215 m above the surface of the southern lowland (Clibbon and Bergeron, 1962).

Historical climate data indicates a mean annual temperature of −0.8 °C (−17.4 °C – 13.8 °C) and mean annual precipitation of 928 mm. Climate projections produced using ClimateNA (Wang et al., 2016) show a likely increase of 23% in precipitation, as well as an increase in minimum temperature of +5.9 °C and maximum temperature of 4.7 °C by the end of the century. These values are averaged across all four shared socioeconomic pathway scenarios of a 13 general circulation model ensemble (Wotherspoon et al., 2022, 2024).

2.2. Data sources

To characterize changes in the forest structure associated to ESB infestations and understand how initial forest structure modulate the severity of ESB infestations, we utilized three data sources: (i) Landsat time series for SR disturbances masking, (ii) FRI data which contain

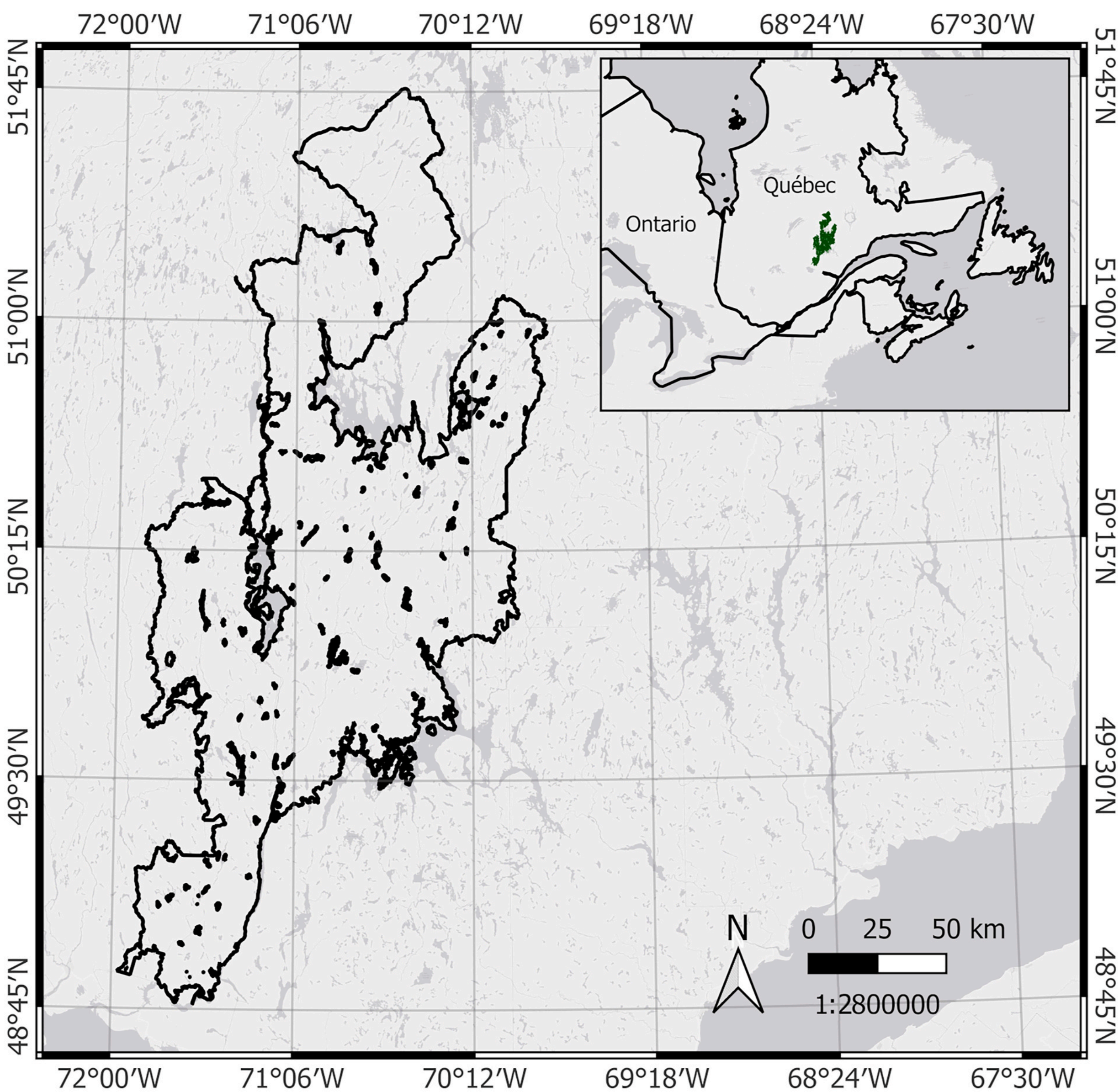

Fig. 1. Map of Lac Saint-Jean, Quebec, Canada. In the inset, black polygons demarcate Canadian provincial boundaries.

photointerpreted information on disturbance type, distribution, and year of occurrence, and (iii) a bitemporal ALS dataset consisting of two acquisitions in 2014 and 2020, all of which are described below.

2.2.1. Disturbance mapping

We utilized the National Terrestrial Ecosystem Monitoring System (NTEMS), which provides a Canada-wide inventory database built from Landsat time series to detect changes in spectral reflectance and characterize annual disturbances at a 30 m spatial resolution (White et al., 2014) based on the Composite2Change approach (Hermosilla et al., 2015). In particular, best available pixel images are produced from Landsat time series using a set of preprocessing functions such as atmospheric correction and cloud masking (White et al., 2014) and a breakpoint detection algorithm (Keogh et al., 2001) detects changes in the Normalized Burn Ratio (Key and Benson, 2006) to characterize disturbances. These annual disturbance layers were used to mask SR fire occurrences (high and low confidence) from 2014 to 2020 and harvesting (high and low confidence) from 1999 to 2020, according to NTEMS nomenclature (Hermosilla et al., 2015).

The second data source we utilized was the provincial FRI from the

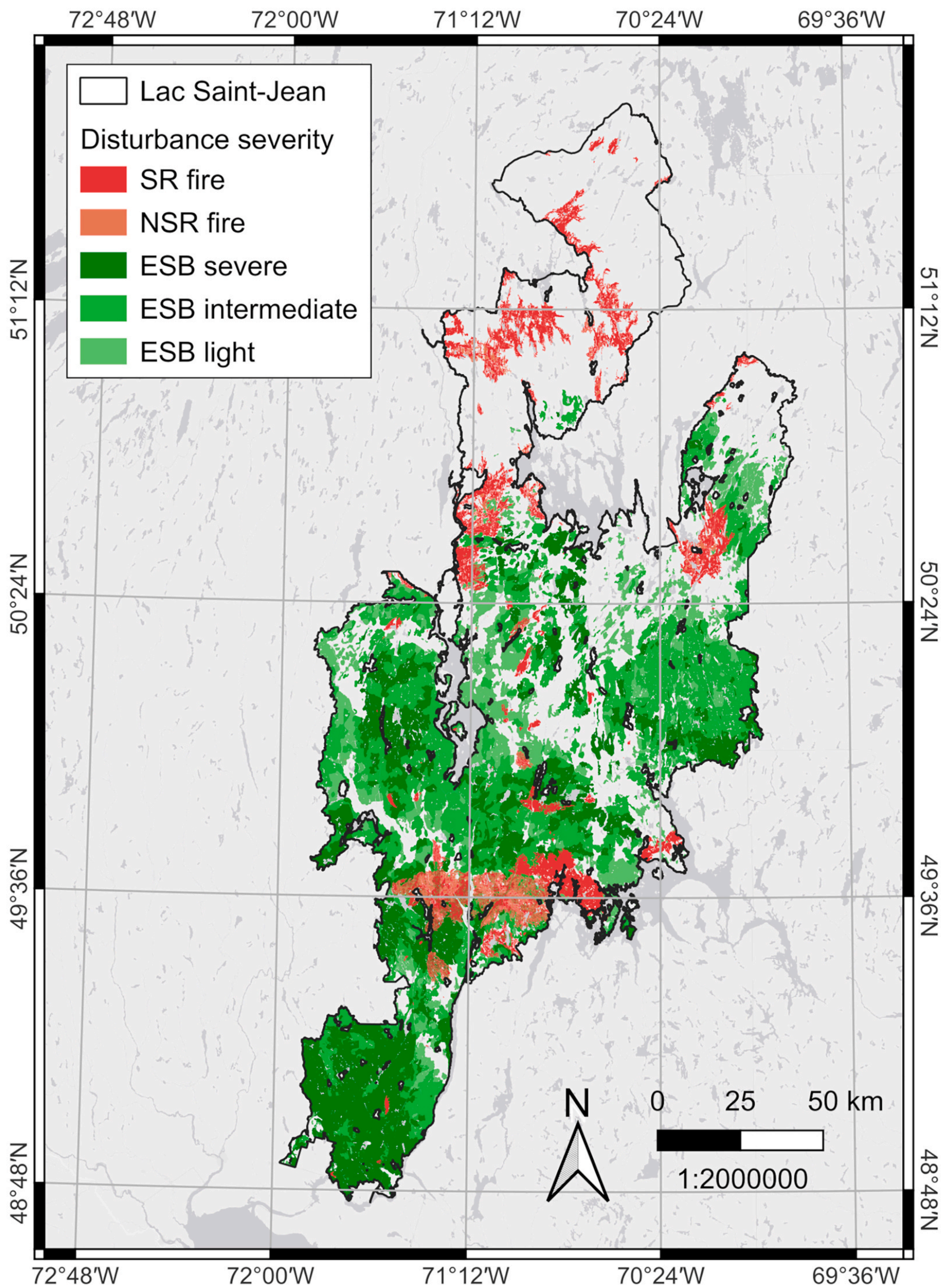

Fig. 2. Map of the distribution of disturbance severity categories as reported by the provincial FRI in the form of polygon layers between 2014 and 2020. Light ESB infestations indicate that the upper 1/3 canopy of few trees is defoliated within a given interpreted polygon. Intermediate indicates upper 1/2 canopy of many trees is defoliated. Severe indicates full canopy defoliation of many trees. NSR fires indicate between 25% and 75% tree removal. SR fire indicates full tree removal.

Quebec Ministère des Ressources naturelles et des Forêts, which provides more granular disturbance information than NTEMS, allowing us to distinguish varying ESB infestation severity. The provincial FRI compiles annual occurrences of forest disturbances and interventions, including harvesting and planting in the form of vector layers at a minimum mapping unit (MMU) of 0.1 ha. The FRI uses a combination of interpreted aerial photos, satellite imagery, and annual reports, whereas other inventory information are updated at 10-year cycles through photointerpretation and sampling plots. The major disturbances mapped in the FRI include, ordered by area, ESB outbreaks, wildfires, diseases, windthrows, and frost damages. In particular, wildfires and ESB outbreaks are further categorized based on the disturbance extent and severity (Fig. 2). The total area affected by SR and NSR wildfires from 2014 to 2020 amounted to approximately 20,000 ha and 30,000 ha, respectively (Ministère des Ressources naturelles et des Forêts, 2023b), while ESB defoliations amounted to approximately 2.55 million ha (Ministère des Ressources naturelles et des Forêts, 2023a).

A cumulative severity map integrating annual disturbance information from 2014 to 2020 was developed by first rasterizing the annual vector layers of ESB infestations from the provincial FRI to 10 m with each severity class labelled as 1–3 and then summing the annual disturbance raster products. Harvesting and planting activities were masked as were roads and water bodies with a 20 m buffer using downsampled NTEMS to 10 m and provincial layers. Upon masking, only areas infested by cumulative ESB infestations remained. Lastly, isolated cumulative severity pixels were removed using a MMU of 1 ha and a perimeter-area ratio of 0.5 filters.

2.2.2. Aerial laser scanning dataset

We obtained two discrete return ALS acquisitions in 2014 and 2020 in the southernmost portion of the LSJ region over an area of approximately 2893 km^2. Table 1 details the acquisition specifications for the two datasets. The 2014 acquisition was scanned between June 22nd and September 27th with an Optech ALTM Gemini at 1200 m above ground level (AGL) with an effective average point density of 3.4 points m^{-2}. The 2020 Riegl VQ-1560i acquisition was scanned at 1600 m AGL between August, 14th and September 25th and had an effective point density of 13.6 points m^{-2}.

3. Methods

The methodology applied in this research is summarized in Fig. 3 and described in detail in the following sections.

3.1. Aerial laser scanning data processing

3.1.1. Georeferencing

Point cloud data is subject to georeferencing errors due to geometrical distortions associated with the coordinate reference systems used (Zhang and Shen, 2013), inaccurate system calibration, and measurement errors of the laser itself (White et al., 2013). Therefore, it is important to verify the correct registration of overlapping point clouds to perform accurate change detection and characterization. To do so, the point clouds were first harmonized by applying the same coordinate scale and offset to match the lower precision acquisition in 2014 and projecting both datasets to a common coordinate reference system (EPSG:2949). Point cloud vertical and horizontal registration, as well as classification, were performed by the data providers. However, we checked the quality of the registration using an iterative closest point algorithm (Besl and McKay, 1992) on 1000 tiles covered by the road network, and we randomly sampled 100,000 ground points on the roads for each tile. The use of ground returns on the road network allowed us to remove the effect of canopy cover from the results of the registration. We observed marginal vertical and horizontal offsets between the two point clouds with a root mean square error (RMSE) of 8.5 ± 7 cm for the vertical alignment, 10.2 ± 4 cm for the horizontal alignment along the x axis, and 10.8 ± 4.8 cm along the y axis.

Table 1
Summary of the bitemporal ALS acquisition specifications.

Specifications	ALS – 2014	ALS – 2020
Sensor type	Optech ALTM Gemini	Riegl VQ-1560i
Pulse repetition frequency	100 kHz	700 kHz
Scan angle	±15°	±20°
Wavelength	1064 nm	1550 nm
Average flight altitude (AGL)	1200 m	1600 m
Nominal average point density	2.3 points m^{-2}	2.5 points m^{-2}
Effective average point density	3.4 points m^{-2}	13.6 points m^{-2}
Spatial extent	11,230 km^2	3401 km^2
Overlapping area	2916 km^2	

3.1.2. Normalization

Point cloud normalization is fundamental to remove the effect of topography from change detection and characterization. Prior to normalization, we removed duplicate points with identical GPS locations along the x, y, and z axes due to flight line overlaps and multi-return sensors used (Isenburg, 2024). Noise points in clusters of 10 or fewer within a 3 m voxel were also filtered using a distance-based noise filtering algorithm (Isenburg, 2024). Point cloud normalization was conducted using a DTM generated from the higher-density 2020 ALS acquisition via a Triangulated Irregular Network interpolation (TIN) at a 1 m spatial resolution. A TIN algorithm was selected for its robust terrain approximation capabilities with buffered ALS tiles to avoid edge artifacts and high processing speed even with large data volumes. Flight line overlaps were removed after normalization at a 0.5 m step. All ALS processing steps were carried out via a combination of LAStools (Isenburg, 2024) and lidR (Roussel et al., 2020).

3.2. Metrics extraction and quantification of change

We computed 14 ALS metrics rasterized at 10 m spatial resolution for both point clouds with a MMU of 500 m^2, which were then subtracted over time ($t_2 - t_1$) (hereafter delta metrics) (Table 2). Collinearity analysis of the delta metrics revealed no correlation using a Pearson's correlation coefficient of 0.8, which is considered to be indicative of very strong correlations in various disciplines (Akoglu, 2018). The delta metrics were estimated under disturbed conditions only as the focus is on the characterization of structural changes resulting from ESB infestations. The delta metric selection was cognizant of the expected variations in the forest structure caused by ESB attacks, typified by variations in mid-to-upper tree height, canopy cover, canopy permeability, and canopy structural complexity (Atkins et al., 2020). For instance, it is expected that insect defoliations target the mid-upper canopy, decrease canopy cover and increases light penetration depending on the severity and time since the attack (Bouchard and Pothier, 2010). In summary, the 14 selected delta metrics can be divided into three categories. The first category includes changes in height metrics as height percentiles and cumulative height. Tree top information were excluded as they are not expected to vary significantly as a direct result of ESB attacks. The second category includes changes in canopy metrics such as canopy cover above 2 m (White et al., 2013), gap fraction at 5 m as a measure of light penetration, and LAI above 2 m (Bouvier et al., 2015). These metrics capture canopy permeability and light reception useful to describe insect defoliations (Bouchard and Pothier, 2010). The selection of the height cut-off thresholds allowed us to exclude the effect of ground and below-canopy returns in the characterization of structural changes (White et al., 2013). In particular, we experimented with the gap fraction profile threshold and selected a 5 m cut-off value corresponding to the height at which we could capture the greatest pixel-level variability in light penetrability across the study area. Ultimately, experimenting with height thresholds would permit to better capture a larger portion of variability in site conditions and derive

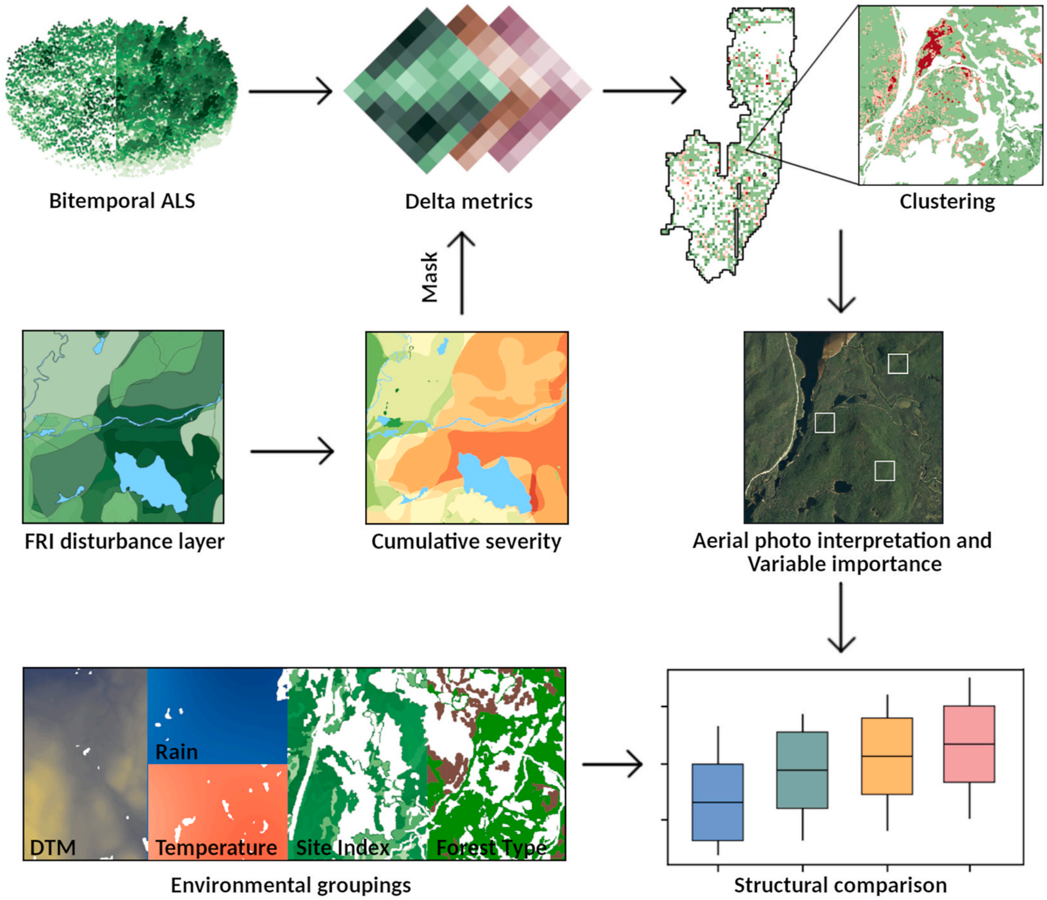

Fig. 3. Illustration of the methodological flow of the study.

Table 2
Overview of the ALS metrics extracted in this study.

Category	Notation	Definition
Height	p25 – 50–75 (m)	25th – 50th – 75th height percentile
	pcum40 – 60 (%)	Cumulative height at p40 – 60
Canopy	Cover (%)	Canopy cover above 2 m (z) using all returns (R) $R_z/R_{tot} \times 100$
	Gap	Gap fraction profile at 5 m (z) at 1 m intervals (dz)[a] $\sum_{i=0}^{n} R_{[0:z]} / (R_{tot} - R_{[0:z+dz]})$
	LAI	LAI above 2 m with extinction coefficient (k) of 0.5 [a] $\sum_{i=0}^{n} - log\,(Gap_i)/k$
Eigen	$\lambda_{1,\,3}$	Largest and smallest eigenvalues
	Eccentricity	Eccentricity of the covariance matrix[c] $log(\lambda_1 / \lambda_2)$
	Planarity	Plane-like shape of a point group[c] $(\lambda_2 - \lambda_3)/\lambda_1$
	Sphericity	Sphere-like shape of a point group[c] λ_3/λ_1
	Anisotropy	Variance spread between eigenvectors for a point group[c] $(\lambda_3 - \lambda_1)/\lambda_3$

[a](Bouvier et al., 2015), [b](Mallet et al., 2011), [c](West et al., 2004)

more representative structural metrics (Nyström et al., 2012; White et al., 2013). The third category are changes in eigen-based metrics calculated from covariance matrix eigendecomposition of the point cloud within a pixel (Lucas et al., 2019). Eigendecomposition refers to the factorization of a matrix into eigenvalues and eigenvectors which may be used to describe the spatial configuration of ALS returns (Lucas et al., 2019). In this study, the local structure tensor, defined by the x, y, and z coordinates of points within a pixel was used to build a covariance matrix and rank the three corresponding eigenvalues ($\lambda_1 > \lambda_2 > \lambda_3$) for all points above 2 m. The magnitude of the eigenvalues describes the variance of points along perpendicular eigenvectors. Hence, they are informative in that they can detect 3D shapes or estimate temporal changes in spatial configuration of points (Hackel et al., 2016; Lucas et al., 2019; Mezey and Houle, 2003; Milocco and Salazar-Ciudad, 2022; Steppan et al., 2002). Previous studies have addressed the use of eigen-based features for the segmentation of linear and regular features at sub-meter level (Hackel et al., 2016; Lucas et al., 2019). However, these studies have mostly worked with well-defined geometries or aimed to segment features into broad categories (e.g. vegetation/non vegetation). We opted for a larger point neighborhood to better capture changes in the spatial configuration of small groups of trees that would otherwise be more challenging to observe in sub-meter neighborhoods, and evaluate if sacrificing these small-scale variations may still offer novel insights into structural changes related to ESB infestations.

3.3. Structural change characterization

We applied a two-stage clustering approach consisting of an initial kmeans pass (Lloyd, 1982; MacQueen, 1967) to partition the 14 delta metrics into 100 pre-clusters, followed by multivariate agglomerative clustering (Murtagh and Contreras, 2012). Multivariate agglomerative clustering is one of the most commonly used methods to derive clusters representing ecological regionalizations (Snelder et al., 2010) and has been successfully applied in previous literature exploring cluster analysis on metrics of ecological importance (Coops et al., 2009, 2020; Guo et al., 2017; Hargrove and Hoffman, 2004). Furthermore, delta metrics were scaled to their 5–95 interquartile range and median-centered to provide a more robust standardization measure to data outliers. To remove multivariate noise, a Principal Component Analysis (Jolliggr,

2002) with three components explaining 99% of variance was fit to the data. We observed that 99.8% of data was within the interquartile range of both principal components and we removed observations that were outside that range.

The kmeans pre-clusters were initialized 1000 times with a kmeans++ initializer (Arthur and Vassilvitskii, 2007) and the multivariate agglomerative clustering with a Ward's linkage function (Ward, 1963) was run on the pre-clusters to focus on a smaller number of numerically-representative and hierarchically-organized response patterns. A logical dendrogram cut-off at a 30% scaled distance resulted in a final selection of 6 clusters. The Manhattan distance was selected for clustering because it is more robust in higher dimensional spaces where other distance metrics (e.g. Euclidean) become less informative due to sparser data distribution (Aggarwal et al., 2001). To address residual variability in the resulting clusters, a 3×3 modal filter was applied to retain only the majority cluster. A fraction of cluster regions smaller than 500 m^2 were either merged with neighboring cluster or removed if isolated.

Cluster separability in relation to the delta metrics and cumulative disturbance severity was assessed using a Kruskal-Wallis rank sum test (Acar and Sun, 2013) and a two-sided Dunn's post-hoc multiple pairwise comparison test (Dunn, 1964) with a Sidak correction to control for error among multiple comparisons (Sidak, 1967) on a randomly shuffled data subsample of 5000 pixels per cluster, similarly to previous research conducting cluster analysis on variables of ecological importance (Guo et al., 2017; Smith-Tripp et al., 2024). To further examine clustering separability based on the delta metrics and assess variable importance from a modeling perspective (Guo et al., 2017), a random forest classifier (Breiman, 2001) was trained and tuned with a 70-30 split and a 5-fold cross-validation based on the area under the receiver operating characteristic curve (ROC AUC) (Bradley, 1997) on the same subsample. In particular, this step allowed us to treat a subset of the clustered data as truth and compare it to the remaining data points in the subsample after the split, similarly to the methodology proposed by Guo et al. (2017). Parameter tuning was run via a random search in a parameter space of 20,000 elements. In conclusion, a permutation feature importance routine was run on the random forest classifier to determine feature importance with 1000 shuffles based on ROC AUC scores. The cluster analysis was conducted in Python environment.

3.4. Validation of clustered data

To validate our structural change characterization, we looked at how well clusters representing varying cumulative severity matched the severity of ESB attacks on the ground. To do so, we used two available aerial imagery acquired by the Ministère des Ressources naturelles et des Forêts of Quebec in 2012 and 2020 at 20 cm and 30 cm spatial resolution, respectively. The aerial imagery were interpreted by an independent trained photointerpreter across a network of 415 randomly stratified locations based on the final clusters using sgsR (Goodbody et al., 2023). Plot design consisted of two overlapping squared polygons at 100 m^2 and 900 m^2 to capture multiscale variability in forest structural attributes and remove spatial autocorrelation by sampling at a minimum distance of 500 m. The interpretation evaluated the amount of decoloration, defoliation, and gaps in both imagery by assigning an incremental value from 0 (no impact) to 5 (high impact) for each indicator. Ultimately, higher severity clusters are expected to match higher levels of defoliation, decoloration, and gaps on the ground as infestations become more severe over time. However, gaps are not expected to vary as much due to more localized gap-scale mortality dynamics (Bouchard et al., 2006a; Bouchard and Pothier, 2010; D'Aoust et al., 2004).

3.5. Initial forest structure and infestation severity

To understand the role of initial forest structures in modulating the severity of the infestation, we compared forest structures that lead to lower infestation severity to structures that lead to higher infestation severity. The comparison was stratified by areas experiencing similar local environmental conditions (hereafter domains). The use of domains allowed us to disentangle the effect of top-down control factors such as climate, elevation, and forest type from the comparison. Domains were extracted at a 10 m resolution using a kmeans classification with 4 arbitrary clusters on the basis of climate normals between 2000 and 2020 for mean annual temperature and precipitation (Wang et al., 2016), elevation as derived from the 2020 DTM, stand-level site index at 50 years from the FRI, and stand-level forest type (conifer, mixedwood) from the FRI.

The separate distributions of each ALS metrics were extracted for each cluster and compared across all cluster pairs under each domain. For example, canopy cover values were extracted for each cluster that belonged to the same domain, and pairwise comparison were conducted among those clusters. This was done separately for each domain. Comparisons were conducted using a Kruskal-Wallis test (Acar and Sun, 2013) on a randomly selected subset of 1000 pixels per cluster. In particular, we considered that a statistically significant differences between a low and high severity cluster comparison would signify that the compared structural attribute (e.g. canopy cover) had a role in modulating the severity of the infestation under that specific domain.

4. Results

Structural changes due to ESB were characterized broadly, with spatial aggregations observed throughout the region for clusters representing low and high cumulative severity. The mapped location of the clusters is shown in Fig. 4. Cluster 1 represented the lowest cumulative severity and was predominant in southern LSJ extending for some 1000 ha. Clusters 2 and 4 were mostly present in southern regions covering the approximately 22,000 ha and 14,500 ha, respectively and represented areas with low cumulative severity. Cluster 3 representing intermediate cumulative severity had a widespread distribution and covered the largest extent of 85,000 ha. Clusters 5 and 6 captured high cumulative severity and presented spatial aggregations in the northernmost part of LSJ, as well as south-eastern regions. These clusters were small in extent each covering approximately 2000 ha. Low severity clusters mostly occurred under conifer forests, whereas mid-to-high severity clusters 4–6 were mostly located under mixed forests. Fig. 5 illustrates the distribution of the clusters in relation to cumulative disturbance severity. The statistical tests ran to check overall and pairwise cluster separability returned significant differences (p-value <0.001) for both the Kruskal-Wallis and Dunn's tests.

4.1. Structural change characterization

The structural changes associated with the clusters returned statistical significance for all ALS metrics (p-value <0.001) based on a Kruskal-Wallis followed by a Dunn's post-hoc test. Non-significant statistical differences were observed for only 5 pairwise comparisons out of 209 (2.4%, p-value ≥ 0.05) (Fig. 6). Non-significant pairwise comparisons occurred mostly between clusters 3 and 4 for the delta largest and smallest eigenvalues, and sphericity. Canopy cover decreased as cumulative severity increased in clusters 4–6 (−15%, −12%, −6%). Likewise, LAI decreased by approximately 0.5–1 within the same clusters. Gap fraction at 5 m had the largest increase in cluster 6 (+4%) given the loss in canopy cover, followed by cluster 5 (+3%), while it reduced by 5% in cluster 1. Sphericity and anisotropy increased in clusters 1 and 6, whereas decreased from clusters 2–6. We observed growth in upper canopy strata represented by p75 across all clusters, particularly cluster 1, of 0.6 m on average, yet the growth reduces as cumulative severity increases. Conversely, p25 and p50 decreased as cumulative severity increased. Delta p25 decreased by 1.5 m in cluster 6, while changes in p50 were smaller and increased by 1.5 m in cluster 1. Cumulative height

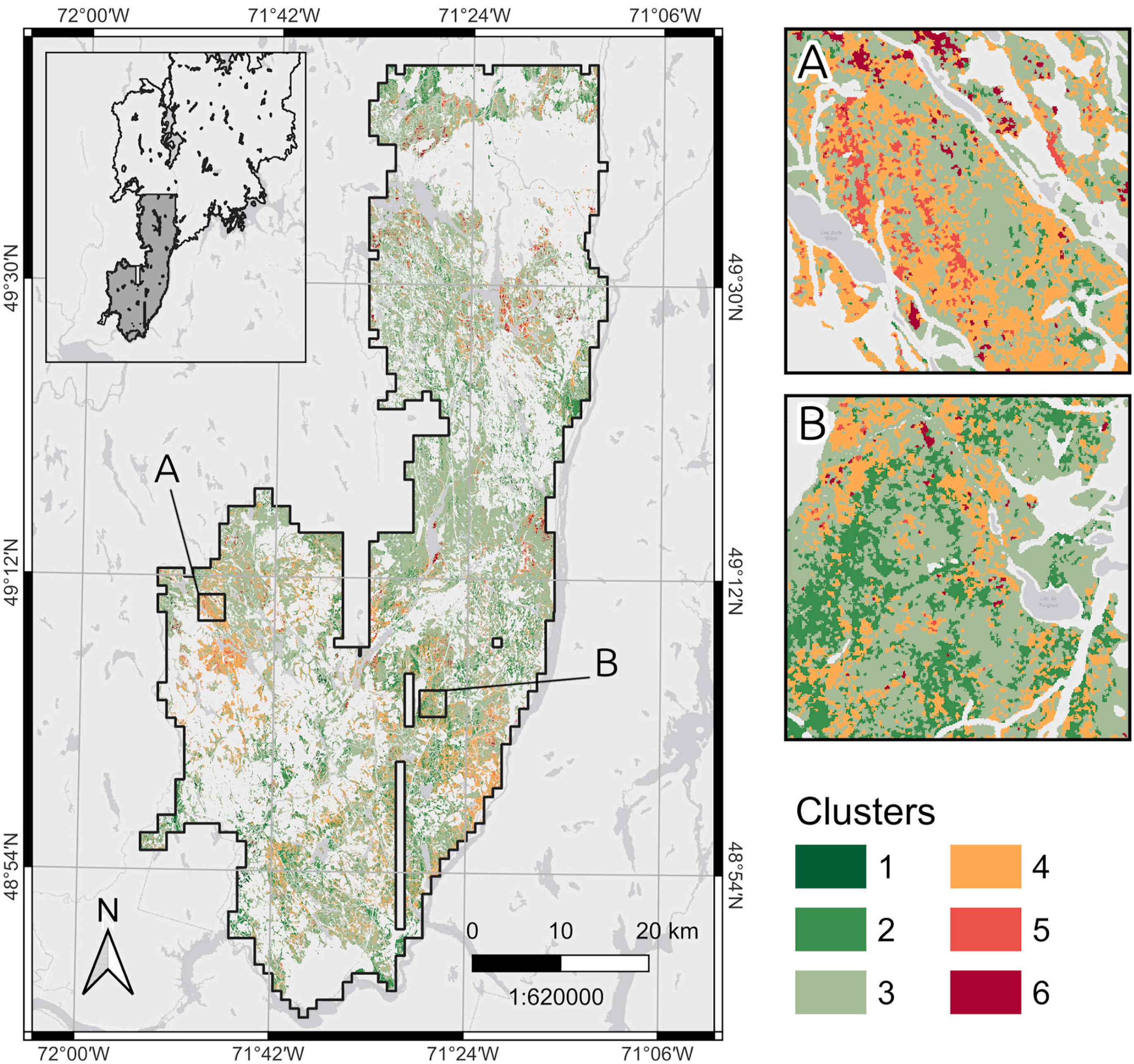

Fig. 4. Wall-to-wall distribution of the six structural clusters derived from the bitemporal ALS acquisition (2014–2020) available in the LSJ region, with a detailed view on A and B for better visualization.

at p40 and p60 decreased in low severity clusters 1 and 2, while increased as cumulative severity increased, up to +15% for p40 under cluster 5.

4.2. Cluster separability assessment

We found that the three most important features for the identification of the 6 clusters based on cumulative severity were the canopy cover, p75, and p25, with a scaled importance of 100%, 74%, and 66% (Fig. A1). It follows the largest eigenvalue with a scaled importance of 59%. Canopy cover showed a distinct response pattern to increasing cumulative disturbance severity, whereas we observed smaller changes in p75 and greater changes in p25 across all clusters.

The confusion matrix of the random forest model used to assess cluster separability and extract variable importance from a modeling perspective is reported in Table A1 and illustrated in Fig. A2. Recall and precision are also reported. Recall indicates the proportion of correctly assigned pixels out of the number of pixels that belong to the positive class. Precision indicates the proportion of correctly assigned pixels out of the total number of pixels labelled as belonging to the positive class. The first most importance source of confusion was between clusters 4 and 5, because they characterize areas with similar cumulative severity levels and have small extents compared to the other clusters. Confusion was also noticed between clusters 3 and 2 for similar reasons. Cluster 1 was the cluster best separated by the random forest classifier followed by clusters 6 and 5.

4.3. Photointerpretation of structural clusters

The aerial photointerpretation conducted at a 100 m^2 plot size to validate the structural characteristics of the six clusters revealed no change in any indicator for cluster 1, representing the lowest cumulative

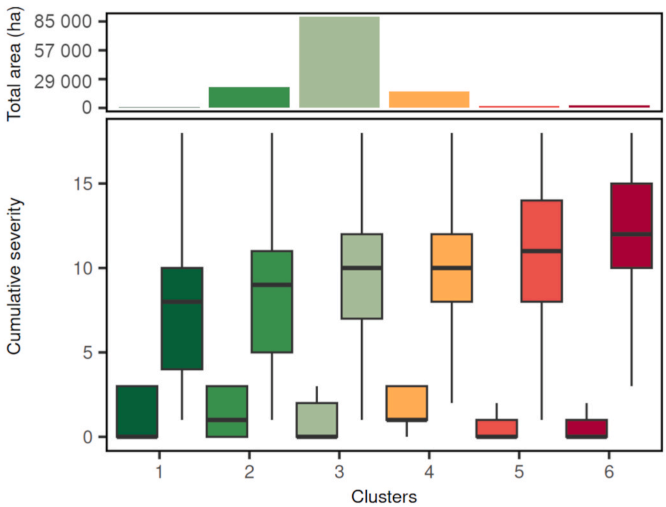

Fig. 5. Distribution of cumulative disturbance severity values, obtained by summing annual ESB severity classes between 2014 and 2020, at the beginning (2014, left) and end (2020, right) of the analyzed period in relation to the six structural clusters derived from the bitemporal ALS acquisition. The total area occupied by cluster is reported in the top panel. Clusters are ordered by increasing mean cumulative severity.

severity. Clusters 2 had a small increase of 0.5 points in decoloration, while defoliation and gaps remained unaltered. Decoloration, defoliation, and gaps continuously increased in clusters representing higher cumulative severity, with cluster 6 having the greatest change in decoloration and defoliation (+2 points, +1 point). Gaps remained relatively stable over time compared to the other indicators. Denser canopies were observed more frequently in high severity clusters than lower severity clusters. Similar findings were observed for the 900 m^2 plots. In general, smaller changes in defoliation and gaps were found in each cluster compared to decoloration. Results of the interpretation for the 100 m^2 plots, along with the relative change of the three most important structural metrics are shown in Fig. 7. In conclusion, the unique cumulative severity, structural, and photointerpreted characteristics associated to each cluster are summarized in Table 3.

4.4. Initial forest structures

4.4. Assessment of initial forest structures

The four domains used to assess the role of initial forest structures in modulating the severity of the infestation are shown in Fig. 8. Within each domain, low and high cumulative severity clusters, represented by clusters 1 and 2, and 5 and 6, respectively, had significantly different distributions (p-value $\leq$0.05) for all three structural metrics (Fig. 9). Clusters 1–3 were characterized by an average canopy cover lower than 65% under domains at lower elevation with warmer and dryer climates. Conversely, clusters 5–7 had initial canopy cover higher than 75% across all domains. Tree height at p75 was shorter for low severity clusters with an average of 3.7 m for cluster 1 and 7.5 m for cluster 2, and taller for high severity clusters at 10.2 m for cluster 5 and 6.6 m for cluster 6, across domains. The value of p25 was lower for clusters 1–3 under domains 2 and 4 with an average of about 1 m compared to 2.3 m for the same clusters under domains 1 and 3. High severity clusters were characterized by an average p25 of 4.5 m across domains.

5. Discussion

Characterizing disturbance events is essential for forest management practices focused on topics such as reporting forest change (White et al., 2017), shifts in forest dynamics towards alternate or novel states (Seastedt et al., 2008), carbon sequestration, or sustainability. While SR disturbances have been previously detected and attributed in Canadian forests (Hermosilla et al., 2015), NSR disturbance are more challenging to characterize, and the mechanisms involved in influencing the forest structure remain elusive (Kneeshaw et al., 2021). In particular, changes resulting from ESB attacks impact the forest structure in more subtle ways than other disturbances such as wildfires. Recognizing these limits, we took an exploratory and data-driven approach, whereby we characterized changes in the forest structure associated to ESB attacks based on changes in a bitemporal ALS dataset. This paper offers new insights into ESB infestation dynamics by synthesizing the changes in structural characteristics associated to attacks of varying severity and assessing the role of initial structures in modulating the severity of the infestation.

5.1. Initial forest structures modulate infestation severity

Canopy cover, p75, and p25 were the three most important metrics in separating the clusters and revealed a consistent response pattern to increasing infestation severity. In particular, canopy cover was the most important structural metric to characterize ESB attacks, in line with previous research (Bouchard et al., 2006a; Bouchard and Pothier, 2010; D'Aoust et al., 2004). Canopy cover and tree height are some of the most readily observable metrics from lidar. Consequently, it is logical that these metrics were the most sensitive to separating the clusters. These are also directly interpretable metrics of change, making them suitable indicators for inclusion in silvicultural strategies aimed at NSR disturbance management (Senf et al., 2017).

We evaluated these metrics at the beginning of the ALS acquisition period to assess which structures had the greatest role in modulating ESB infestation severity. We observed that the initial canopy cover, associated to larger canopy gaps, was lower in low severity clusters with an average < 65% across all domains compared to denser higher severity clusters above 75%. The distribution of cover values in clusters 1–3 was also significantly different to the distributions in clusters 4–6 for all domains. The association between initial lower canopy cover and higher canopy openness promotes more vigorous crowns which, in turn, result in a lower susceptibility to ESB infestations (Kneeshaw et al., 2021; Virgin and MacLean, 2017). Therefore, we suggest that the lower infestations severity at the end of the analyzed period is a joint result of an initial lower canopy cover and larger gaps which promoted more vigorous, less susceptible trees, irrespective of the domain. Similarly, p75 and p25 were shorter for clusters 1–3 than higher severity clusters 4–6 across all domains. Smaller differences were observed for p75 than p25, especially for clusters 2–5 under domains 1 and 3. These were domains that occurred in southern areas and underwent severe infestations only before 2016. They were also characterized by higher elevation above 400 m, mean annual precipitation above 975 mm, lower mean annual temperature below 1 °C, and the lowest site index below 14 m at 50 years. There, the structural influence on infestation severity seemed to be less a result of lower tree height at p75. Hence, a lower infestation severity in these clusters may be partially driven by environmental conditions less favorable for the infestation, rather than differences in forest structures (Robert et al., 2018; Royama, 1984). In domains where conditions were not as limiting for outbreaks to occur, shorter trees at p75 suggest lower ESB infestation severity. Distribution of p25 values indicate that, irrespective of the domain, shorter canopies at p25 rendered lesser severe infestations for similar reasons highlighted for canopy cover and p75.

In summary, we have observed that, where environmental conditions were not limiting for an infestation to outbreak, sparser canopies with low initial canopy cover and shorter trees measured p75 and p25 rendered less severe ESB infestations. In particular, the lowest infestation severity was achieved with canopy cover <65%, p75 < 2.5 m, and p25 < 7.5 m. Instead, the highest infestation severity was achieved with canopy cover >75%, p75 > 10 m, and p25 > 4.5 m. These results indicate the importance of initial canopy cover and tree height in modulating infestation severity, and provide further evidence that more open stands show lower susceptibility to ESB infestations (Kneeshaw

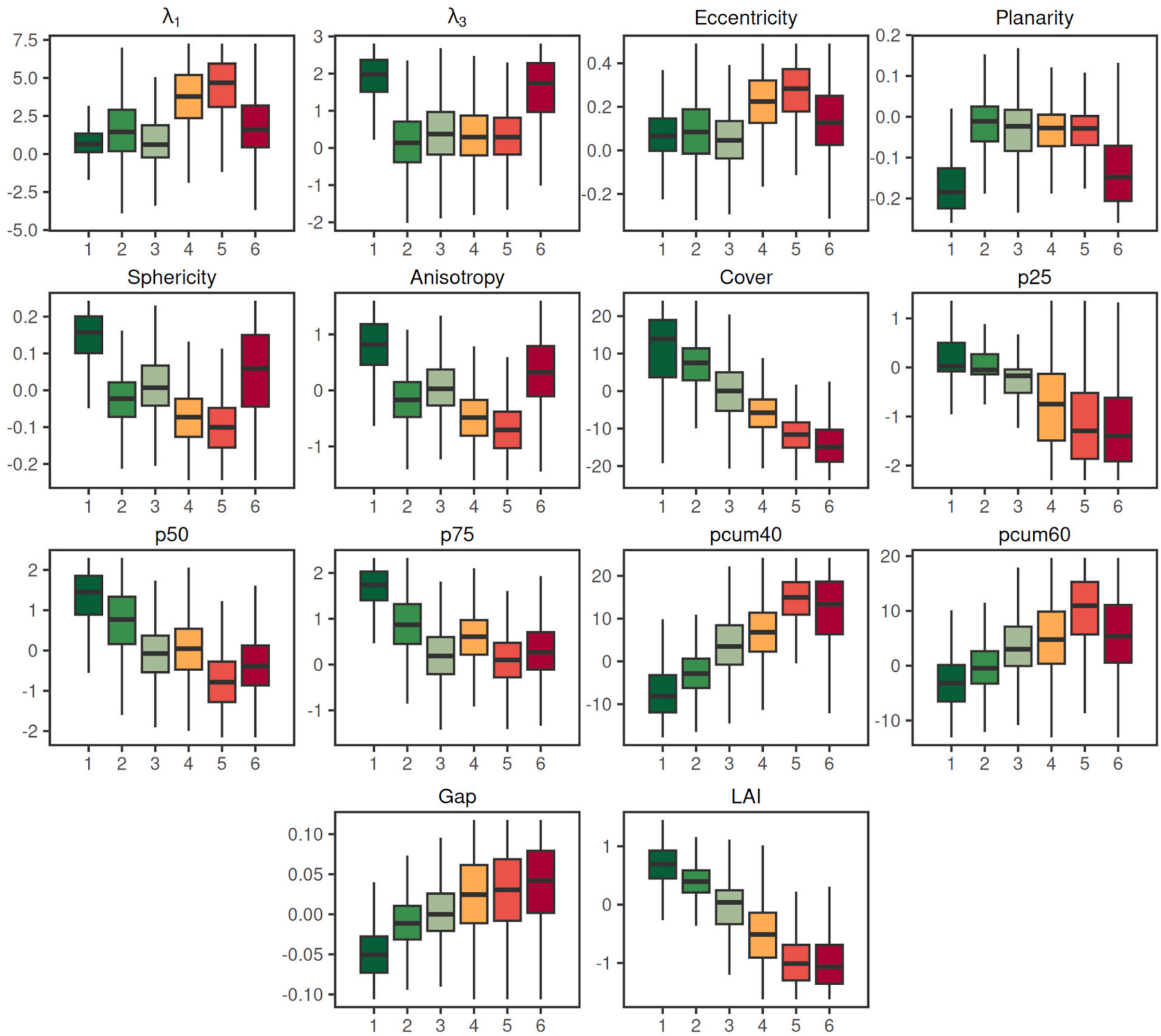

Fig. 6. Distribution of 14 delta metrics by structural cluster derived from the bitemporal ALS acquisition (2014–2020). Values larger than 1.5 times the interquartile range for each metric were removed. Clusters are order by increasing mean cumulative severity, obtained by summing annual ESB severity classes between 2014 and 2020.

et al., 2021; Virgin and MacLean, 2017).

5.2. Forest structural changes are driven by canopy cover and height

Our structural change characterization was subject to a four-fold increase in point density from the first to the last ALS acquisition. Variations in points density over time may affect a correct change characterization if the metrics used for the characterization show great sensitivity to varying densities. To alleviate this issue, we used a raster differencing approach combined with a two-stage cluster analysis. We found that this approach was effective at characterizing changes associated to ESB infestations at fine scale despite variations in point densities between ALS acquisitions. Moreover, canopy cover estimates at high point densities have shown to be comparable to estimates derived at lower densities of around 1 point m^{-2} (Ma et al., 2017). Conversely, height derivations are more sensitive to variations in point density. Therefore, we avoided tree top estimations in favor of mid-to-upper tree height estimates, which are expected to be as well representative of structural changes associated to ESB attacks (Atkins et al., 2020).

We observed increases in canopy cover and p75 associated with the low infestation severity. Light attacks affect only portions of the canopy and single events do not generally render tree mortality (Candau and Fleming, 2005; Virgin and MacLean, 2017). While repeated infestation cycles may subsequently kill host species or reduce growth (Bouchard et al., 2006a; Bouchard and Pothier, 2010), light attacks observed at the pixel level may be masked by neighboring non-host tree species growth (e.g. hardwood), or even stimulate growth due to canopy release. Similarly, canopy cover increased for low severity clusters yet decreased as expected in high severity clusters due to repeated high severity infestations which started between 2015 and 2016 in northern areas. Conversely, p25 showed a consistent decrease as infestation severity increased, except for clusters 1 and 2 where small increases were observed. ESB infestations are known to target mid-to-upper canopy strata, yet short canopies may be affected in the presence of high infestation severity (Ghent, 1958; Nie et al., 2018; Ruel and Huot, 1993; Virgin and MacLean, 2017). High recruitment rates of balsam fir and white spruce in LSJ may explain the decrease in p25 in areas where such regeneration was targeted and mortality occurred due to repeated infestations or competition (Nie et al., 2018; Virgin and MacLean, 2017).

There remain limitations associated with information loss during 3D data flattening in the raster differencing method. To address these limitations, we explored the integration of shape metrics derived from covariance matrix eigendecomposition (Hackel et al., 2016; Lucas et al., 2019; West et al., 2004) to transfer 3D geometrical canopy attributes,

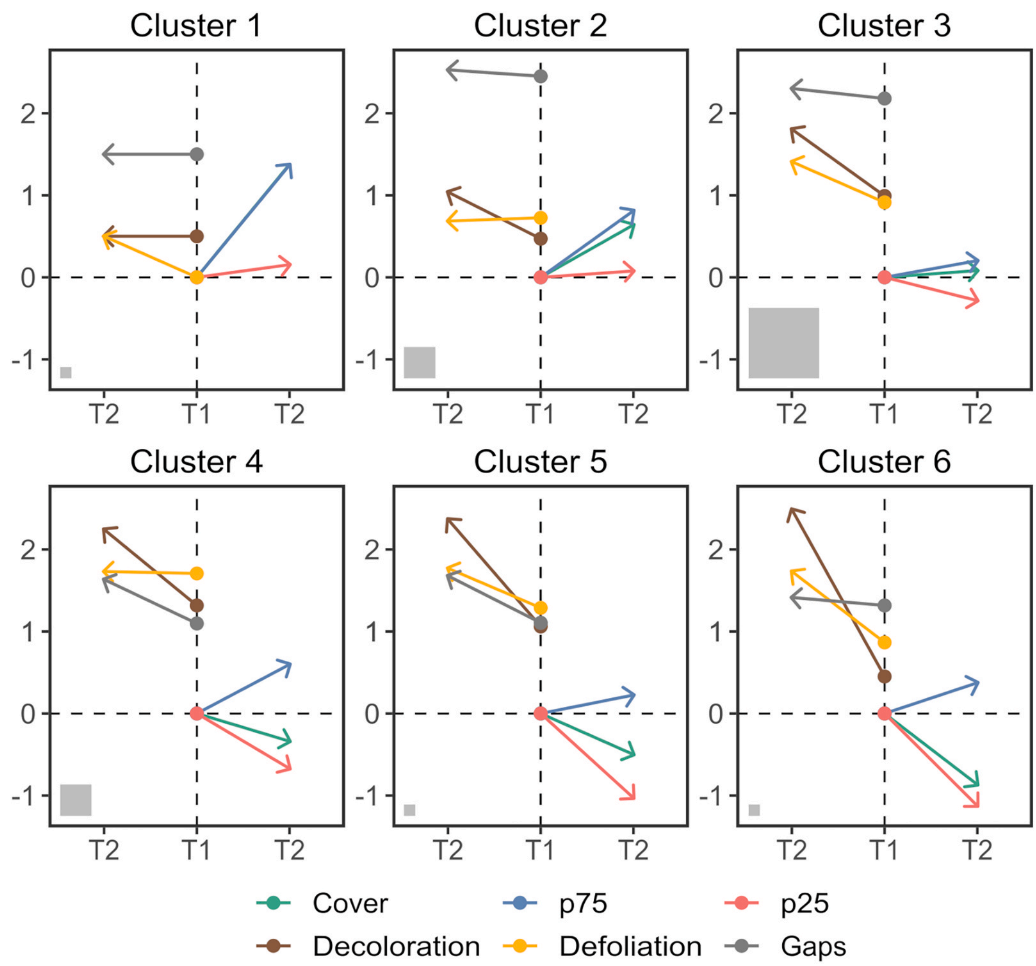

Fig. 7. Temporal changes in structural metrics (cover, p75, and p25) and photointerpreted indicators (decoloration, defoliation, and gaps) by structural cluster derived from the bitemporal ALS acquisition (2014–2020). The left quadrants represent the absolute difference between T1 and T2 for the photointerpreted indicator by cluster. The right quadrants the relative difference for the structural metrics. Grey squares are indicative of the area covered by each cluster. Canopy cover values were divided by 10 for displaying purposes.

Table 3
Summary of the characteristics associated with each cluster in terms of cumulative disturbance severity, change in forest structure between 2014 and 2020, and initial gappiness as reported by the photointerpretation. Changes in forest structure are reported in terms of canopy cover and height (i.e. lower canopy – p25, upper canopy – p75).

Clusters	Description
Cluster 1	Lowest severity, greatest increase in canopy cover and height, moderately dense
Cluster 2	Low severity, moderate increase in canopy cover and height, sparse
Cluster 3	Intermediate severity, small changes in canopy cover and height, sparse
Cluster 4	Intermediate severity, moderate decrease in canopy cover and p25, moderate increase in p75, moderately dense
Cluster 5	High severity, great decrease in canopy cover and p25, small changes in p75, dense
Cluster 6	Highest severity, greatest decrease in canopy cover and p25, small increase in p75, moderately dense

specifically in the form of eigenvalues and eigenvectors, into a raster product, thereby optimizing computational efficiency. We did not find eigendecomposition metrics to be important in the separability of the clusters. However, we observed a distinctive response pattern associated to the largest eigenvalue. In particular, an increase in the largest eigenvalue associated with variance distribution along the dominant eigenvector, in this case normal to the ground, was linked to higher cumulative disturbance severity except for cluster 6. Opposite trends were observed for sphericity and anisotropy. The interpretation of these metrics remains challenging in a forestry context with complex forest dynamics, especially when averaged at the pixel level. Moreover, eigendecomposition metrics are subject to changes associated to the direction of the eigenvectors, which may vary in between acquisitions. Nevertheless, these metrics may be valuable to explore given the complexity of the structural responses associated to NSR disturbances (Atkins et al., 2020).

5.3. *Synchronizing infestation severity and structural changes*

We built a cumulative severity map to synchronize bitemporal structural changes with annual occurrences of ESB. Attacks of ESB do not render immediate changes in the forest structure. It generally takes some years for infestations to manifest (Régnière and Nealis, 2007; Royama, 1984; Virgin and MacLean, 2017) or repeated infestations to attain a severity that can be sensed using airborne lidar systems (Goodbody et al., 2018). The use of a cumulative severity map allowed us to synthesize disturbance information from the FRI into a unique data product detailing the location and severity of repeated infestations, which was a valuable alternative to work with given the lack of time series of ALS data associated to ESB infestations.

We observed that areas characterized by higher cumulative severity, as represented by clusters 5 and 6 were spatially clumped and in close

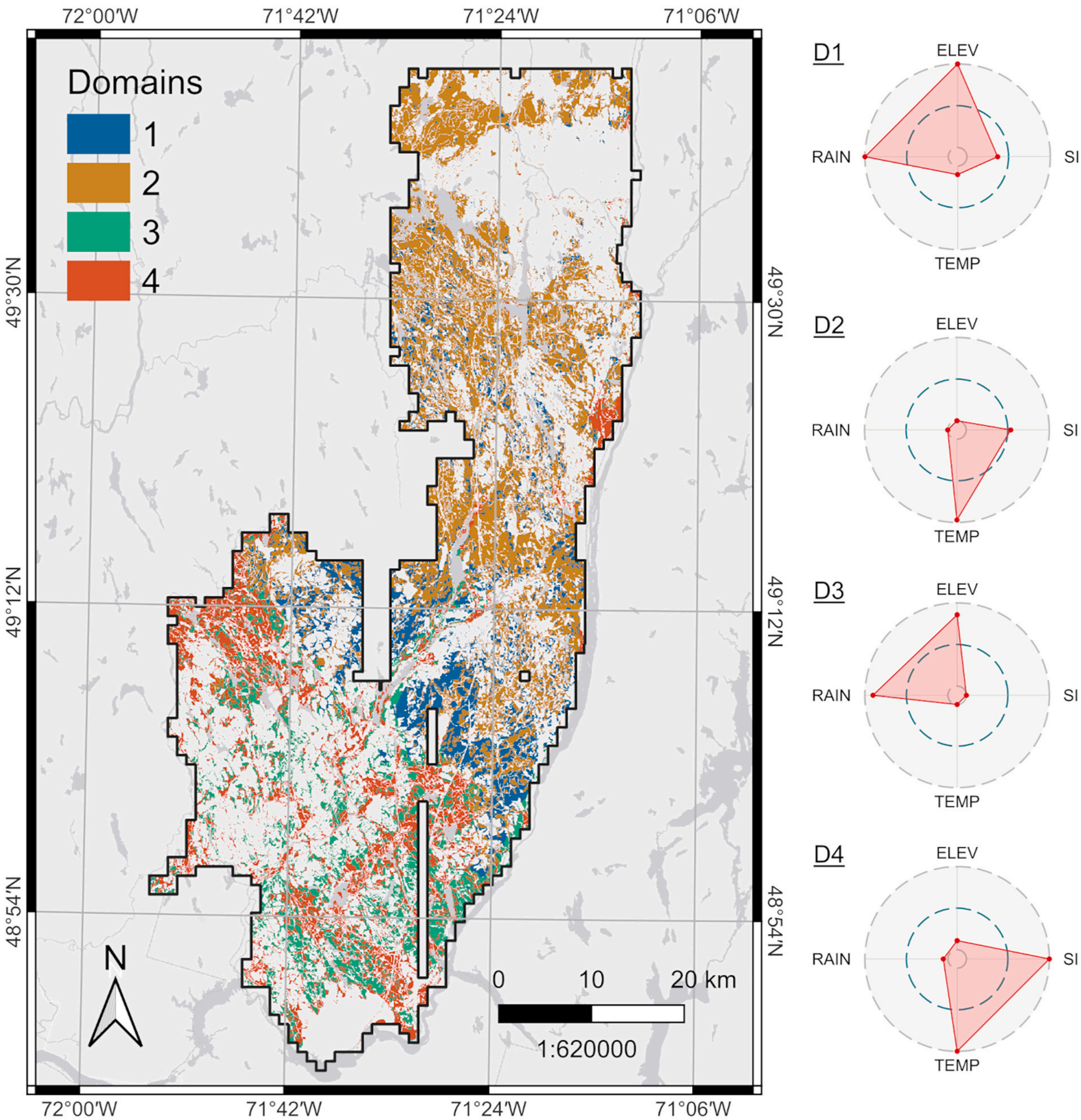

Fig. 8. Map of the distribution of the 4 domains (D) based on the kmeans clustering. On the right, radar plots describing the environmental characteristics of each. Values are scaled 0–1, with the blue dashed line equal to 0.5. D1 and D4 are conifers, D2 and D3 are broadleaves. ELEV = elevation, SI = site index, TEMP = temperature, RAIN = precipitation.

proximity to each other. This observation is consistent with previous literature on the spatial pattern of budworm-related mortality, which is reported to manifest as highly infested trees in a matrix of lighter infestations (Bouchard and Pothier, 2010). These areas were also characterized by closer canopies compared to areas of lower severity. Gaps among canopies were relatively stable between ALS acquisition, despite greater changes observed for high severity clusters, in line with gap-scale mortality as generally reported in the literature (Bouchard et al., 2006a; Bouchard and Pothier, 2010; D'Aoust et al., 2004). In contrast, more open canopies were observed in low severity clusters. Within canopy gaps, as derived from the ALS data, showed greater variability compared to photointerpreted gappiness, which may denote a greater ability of ALS data in informing within canopy dynamics resulting from ESB infestations. High cumulative severity clusters were characterized by repeatedly high severe infestations occurring mostly in northern areas, whereas low severity clusters, predominantly located in the south, were characterized by a few main severe attacks between 2014 and 2016 and then an absence or light infestations in the following years. Moderate infestations were then reported in 2020 for these regions, which may indicate the beginning of a new cycle or delayed canopy decoloration and defoliation observed during the acquisition of new aerial imagery for the FRI (Virgin and MacLean, 2017).

The presence of overlaps in the clusters when assessed against cumulative infestation severity may be attributable to a delayed forest response to ESB attacks (Virgin and MacLean, 2017) or the greater ability of ALS in discriminating and characterizing changes in the forest structure resulting from ESB infestations compared to photointerpretation (Lepš and Hadincová, 1992; Lunetta et al., 1991; Sippel, 1983).

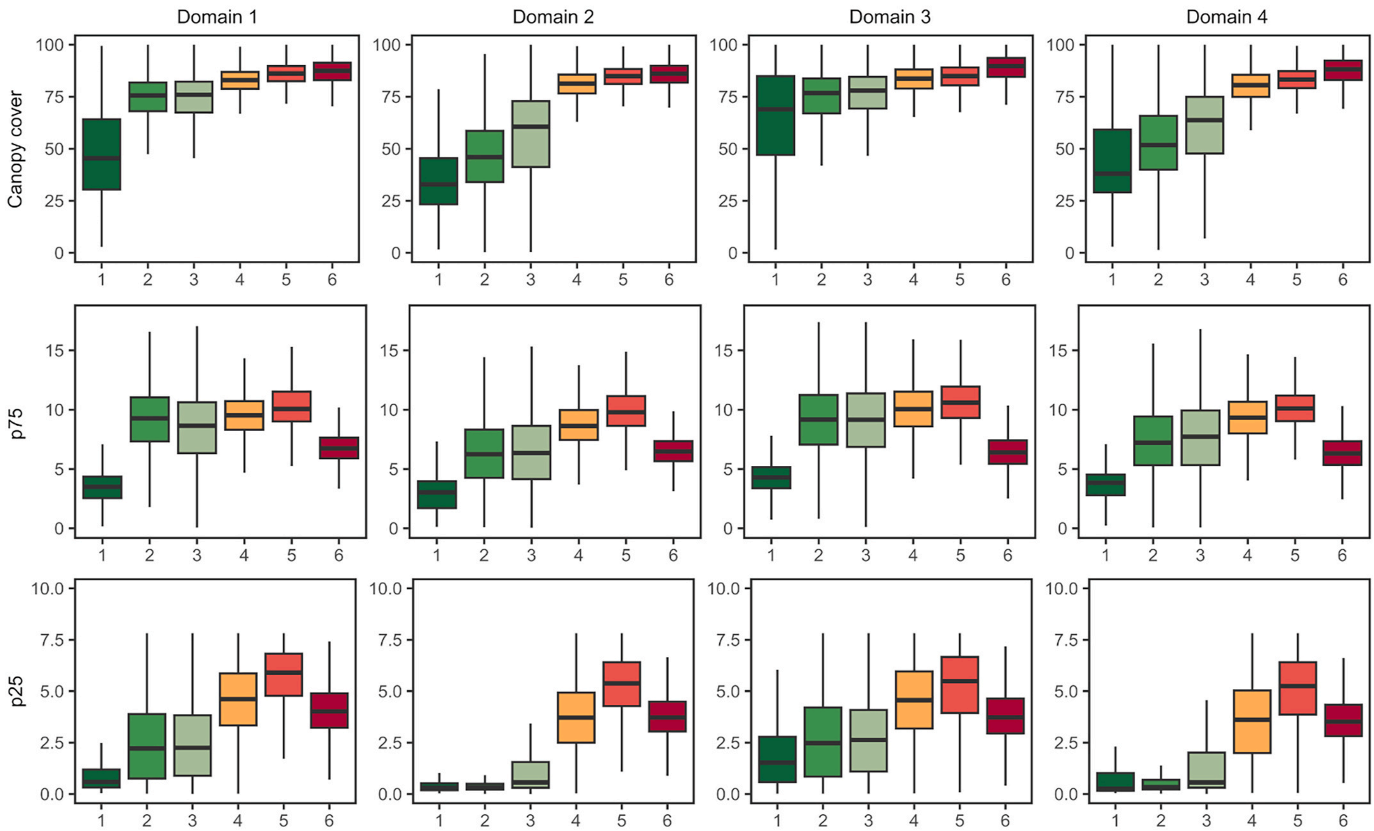

Fig. 9. Distribution of initial canopy cover, p75, and p25 values (2014) by structural cluster, derived from the bitemporal ALS acquisition (2014–2020), under each domain. Distributions associated with low severity clusters 1 and 2 present statistically significant differences to distributions associated with high severity clusters, indicating the role of the ALS metrics in modulating the severity of the infestations. Clusters are order by increasing mean cumulative severity, obtained by summing annual ESB severity classes between 2014 and 2020.

6. Conclusions

The characterization of structural changes at fine scale due to cumulative ESB infestations has potential in regions where bitemporal ALS acquisitions are available. Our study provides a fine-scale wall-to-wall characterization of stands less susceptible to ESB infestation based on canopy cover and height. This information is timely to inform proactive management aimed at maintaining or improving the forest resistance and resilience to ESB infestations in Canadian boreal forests.

Future work on this topic should focus on (i) ground sampling in low severity stands to better understand the relationship between canopy openness, tree vigor, and ESB vulnerability, and (ii) investigating the landscape-level spatial organization of forest structural attributes to understand multiscale structural dynamics linked to ESB.

Funding

This research was funded by a NSERC Alliance project Silva21 NSERC ALLRP 556265-20, grantee Prof. Alexis Achim.

Data availability statement

Airborne laser scanning data is available upon request from the Ministère des Ressources naturelles et des Forêts du Québec.Airborne laser scanning data is available upon request from the Ministère des Ressources naturelles et des Forêts du Québec. The FRI data is available from the Ministère des Ressources naturelles et des Forêts du Québec at https://www.quebec.ca/agriculture-environnement-et-ressources naturelles/forets/recherche-connaissances/inventaire-forestier/donnees-cartes-resultats. The NTEMS data is available at https://open data.nfis.org/mapserver/nfis-change_eng.html.

CRediT authorship contribution statement

Tommaso Trotto: Writing – review & editing, Writing – original draft, Visualization, Software, Methodology, Investigation, Formal analysis, Data curation, Conceptualization. **Nicholas C. Coops:** Writing – review & editing, Writing – original draft, Supervision, Resources, Methodology, Investigation, Funding acquisition, Conceptualization. **Alexis Achim:** Writing – review & editing, Methodology, Funding acquisition, Conceptualization. **Sarah E. Gergel:** Writing – review & editing, Methodology. **Dominik Roeser:** Writing – review & editing, Methodology.

Declaration of competing interest

The authors declare that they have no known competing financial interests or personal relationships that could have appeared to influence the work reported in this paper.

Acknowledgements

This analysis was conducted at the University of British Columbia, which is located on the traditional, ancestral, and unceded land of the xʷməθkʷəy̓əm (Musqueam) people. We thank the anonymous reviewers whose feedback helped to improve and clarify this manuscript.

Appendix A. Supplementary data

Supplementary data to this article can be found online at https://doi.

org/10.1016/j.srs.2024.100160.

References

Acar, E.F., Sun, L., 2013. A generalized Kruskal-Wallis test incorporating group uncertainty with application to genetic association studies. Biometrics 69 (2), 427–435. https://doi.org/10.1111/biom.12006.

Achim, A., Moreau, G., Coops, N.C., Axelson, J.N., Barrette, J., Bédard, S., Byrne, K.E., Caspersen, J., Dick, A.R., D'Orangeville, L., Drolet, G., Eskelson, B.N.I., Filipescu, C. N., Flamand-Hubert, M., Goodbody, T.R.H., Griess, V.C., Hagerman, S.M., Keys, K., Lafleur, B., et al., 2022. The changing culture of silviculture. Forestry: Int. J. Financ. Res. 95 (2), 143–152. https://doi.org/10.1093/forestry/cpab047.

Aggarwal, C.C., Hinneburg, A., Keim, D.A., 2001. On the surprising behavior of distance metrics in high dimensional space. In: Van Den Bussche, J., Vianu, V. (Eds.), Database Theory—ICDT 2001, vol. 1973. Springer Berlin Heidelberg, pp. 420–434. https://doi.org/10.1007/3-540-44503-X_27.

Akoglu, H., 2018. User's guide to correlation coefficients. Turkish Journal of Emergency Medicine 18 (3), 91–93. https://doi.org/10.1016/j.tjem.2018.08.001.

Arthur, D., Vassilvitskii, S., 2007. k-means++: the advantages of careful seeding. Proceedings of the Eighteenth Annual ACM-SIAM Symposium on Discrete Algorithms, pp. 1027–1035.

Atkins, J.W., Bond-Lamberty, B., Fahey, R.T., Haber, L.T., Stuart-Haëntjens, E., Hardiman, B.S., LaRue, E., McNeil, B.E., Orwig, D.A., Stovall, A.E.L., Tallant, J.M., Walter, J.A., Gough, C.M., 2020. Application of multidimensional structural characterization to detect and describe moderate forest disturbance. Ecosphere 11 (6), e03156. https://doi.org/10.1002/ecs2.3156.

Besl, P.J., McKay, N.D., 1992. A method for registration of 3-D shapes. IEEE Trans. Pattern Anal. Mach. Intell. 14 (2), 239–256. https://doi.org/10.1109/34.121791.

Bognounou, F., De Grandpré, L., Pureswaran, D.S., Kneeshaw, D., 2017. Temporal variation in plant neighborhood effects on the defoliation of primary and secondary hosts by an insect pest. Ecosphere 8 (3), e01759. https://doi.org/10.1002/ecs2.1759.

Bouchard, M., Kneeshaw, D., Bergeron, Y., 2006a. Forest dynamics after successive spruce budworm outbreaks in mixedwood forests. Ecology 87 (9), 2319–2329. https://doi.org/10.1890/0012-9658(2006)87[2319:FDASSB]2.0.CO;2.

Bouchard, M., Kneeshaw, D., Bergeron, Y., 2006b. Tree recruitment pulses and long-term species coexistence in mixed forests of western Québec. Ecoscience 13 (1), 82–88. https://doi.org/10.2980/1195-6860(2006)13[82:TRPALS]2.0.CO;2.

Bouchard, M., Pothier, D., 2010. Spatiotemporal variability in tree and stand mortality caused by spruce budworm outbreaks in eastern Quebec. Can. J. For. Res. 40 (1), 86–94. https://doi.org/10.1139/X09-178.

Bouvier, M., Durrieu, S., Fournier, R.A., Renaud, J.-P., 2015. Generalizing predictive models of forest inventory attributes using an area-based approach with airborne LiDAR data. Rem. Sens. Environ. 156, 322–334. https://doi.org/10.1016/j.rse.2014.10.004.

Bradley, A.P., 1997. The use of the area under the ROC curve in the evaluation of machine learning algorithms. Pattern Recogn. 30 (7), 1145–1159. https://doi.org/10.1016/S0031-3203(96)00142-2.

Breiman, L., 2001. Random forests. Mach. Learn. 45 (1), 5–32. https://doi.org/10.1023/A:1010933404324.

Buma, B., 2015. Disturbance interactions: characterization, prediction, and the potential for cascading effects. Ecosphere 6 (4), art70. https://doi.org/10.1890/ES15-00058.1.

Candau, J.-N., Fleming, R.A., 2005. Landscape-scale spatial distribution of spruce budworm defoliation in relation to bioclimatic conditions. Can. J. For. Res. 35 (9), 2218–2232. https://doi.org/10.1139/x05-078.

Choi, D.H., LaRue, E.A., Atkins, J.W., Foster, J.R., Matthes, J.H., Fahey, R.T., Thapa, B., Fei, S., Hardiman, B.S., 2023. Short-term effects of moderate severity disturbances on forest canopy structure. J. Ecol. 111 (9), 1866–1881. https://doi.org/10.1111/1365-2745.14145.

Clibbon, P., Bergeron, R., 1962. Notes on the geology and physiography of the lake saint-jean area, Québec. Cah. Geograph. Quebec 7 (13), 81–100. https://doi.org/10.7202/020420ar.

Cohen, W.B., Yang, Z., Stehman, S.V., Schroeder, T.A., Bell, D.M., Masek, J.G., Huang, C., Meigs, G.W., 2016. Forest disturbance across the conterminous United States from 1985–2012: the emerging dominance of forest decline. For. Ecol. Manag. 360, 242–252. https://doi.org/10.1016/j.foreco.2015.10.042.

Coops, N.C., Shang, C., Wulder, M.A., White, J.C., Hermosilla, T., 2020. Change in forest condition: characterizing non-stand replacing disturbances using time series satellite imagery. For. Ecol. Manag. 474, 118370 https://doi.org/10.1016/j.foreco.2020.118370.

Coops, N.C., Tompalski, P., Goodbody, T.R.H., Achim, A., Mulverhill, C., 2023. Framework for near real-time forest inventory using multi source remote sensing data. Forestry: Int. J. Financ. Res. 96 (1), 1–19. https://doi.org/10.1093/forestry/cpac015.

Coops, N.C., Wulder, M.A., Iwanicka, D., 2009. An environmental domain classification of Canada using earth observation data for biodiversity assessment. Ecol. Inf. 4 (1), 8–22. https://doi.org/10.1016/j.ecoinf.2008.09.005.

D'Aoust, V., Kneeshaw, D., Bergeron, Y., 2004. Characterization of canopy openness before and after a spruce budworm outbreak in the southern boreal forest. Can. J. For. Res. 34 (2), 339–352. https://doi.org/10.1139/x03-278.

Dunn, O.J., 1964. Multiple comparisons using rank sums. Technometrics 6 (3), 241–252. https://doi.org/10.1080/00401706.1964.10490181.

Ghent, A.W., 1958. Studies of regeneration in forest stands devastated by the spruce budworm: II. Age, height growth, and related studies of balsam fir seedlings. - federal Open Science Repository of Canada. For. Sci. 4 (2), 135–146.

Goodbody, T.R.H., Coops, N.C., Hermosilla, T., Tompalski, P., McCartney, G., MacLean, D.A., 2018. Digital aerial photogrammetry for assessing cumulative spruce budworm defoliation and enhancing forest inventories at a landscape-level. ISPRS J. Photogrammetry Remote Sens. 142, 1–11. https://doi.org/10.1016/j.isprsjprs.2018.05.012.

Goodbody, T.R.H., Coops, N.C., Queinnec, M., White, J.C., Tompalski, P., Hudak, A.T., Auty, D., Valbuena, R., LeBoeuf, A., Sinclair, I., McCartney, G., Prieur, J.-F., Woods, M.E., 2023. sgsR: a structurally guided sampling toolbox for LiDAR-based forest inventories. Forestry: Int. J. Financ. Res. 96 (4), 411–424. https://doi.org/10.1093/forestry/cpac055.

Gray, D.R., 2008. The relationship between climate and outbreak characteristics of the spruce budworm in eastern Canada. Climatic Change 87 (3), 361–383. https://doi.org/10.1007/s10584-007-9317-5.

Guo, X., Coops, N.C., Tompalski, P., Nielsen, S.E., Bater, C.W., John Stadt, J., 2017. Regional mapping of vegetation structure for biodiversity monitoring using airborne lidar data. Ecol. Inf. 38, 50–61. https://doi.org/10.1016/j.ecoinf.2017.01.005.

Hackel, T., Wegner, J.D., Schindler, K., 2016. Contour detection in unstructured 3D point clouds. 2016 IEEE Conference on Computer Vision and Pattern Recognition (CVPR), pp. 1610–1618. https://doi.org/10.1109/CVPR.2016.178.

Hargrove, W.W., Hoffman, F.M., 2004. Potential of multivariate quantitative methods for delineation and visualization of ecoregions. Environ. Manag. 34 (1), S39–S60. https://doi.org/10.1007/s00267-003-1084-0.

Hart, J., Kleinman, J., 2018. What are intermediate-severity forest disturbances and why are they important? Forests 9 (9), 579. https://doi.org/10.3390/f9090579.

Hermosilla, T., Wulder, M.A., White, J.C., Coops, N.C., Hobart, G.W., 2015. Regional detection, characterization, and attribution of annual forest change from 1984 to 2012 using Landsat-derived time-series metrics. Rem. Sens. Environ. 170, 121–132. https://doi.org/10.1016/j.rse.2015.09.004.

Isenburg, M., 2024. LAStools. Efficient LiDAR Processing Software (240220 Academic) [C++; Linux]. rapidlasso. http://rapidlasso.com/LAStools.

Jolliggr, I.T., 2002. Principal Component Analysis. Springer-Verlag. https://doi.org/10.1007/b98835.

Keogh, E., Chu, S., Hart, D., Pazzani, M., 2001. An online algorithm for segmenting time series. Proceedings 2001 IEEE International Conference on Data Mining, pp. 289–296. https://doi.org/10.1109/ICDM.2001.989531.

Key, C.H., Benson, N.C., 2006. *Landscape Assessment: Ground Measure of Severity, the Composite Burn Index; and Remote Sensing of Severity, the Normalized Burn Ratio* (RMRS-GTR-164-CD: LA 1-51). USDA Forest Service, Rocky Mountain Research Station. https://pubs.usgs.gov/publication/2002085.

Kharroubi, A., Poux, F., Ballouch, Z., Hajji, R., Billen, R., 2022. Three dimensional change detection using point clouds: a review. Geomatics 2 (4), 457–485. https://doi.org/10.3390/geomatics2040025.

Kleinman, J.S., Goode, J.D., Fries, A.C., Hart, J.L., 2019. Ecological consequences of compound disturbances in forest ecosystems: a systematic review. Ecosphere 10 (11), e02962. https://doi.org/10.1002/ecs2.2962.

Kneeshaw, D.D., De Grandpré, L., D'Orangeville, L., Marchand, M., Moisan-Perrier, J., Robert, L.-E., Bouchard, M., 2022. Forest structure and composition diverge following harvesting compared to a spruce budworm Choristoneura fumiferana (clem.) outbreak. Frontiers in Forests and Global Change 5. https://doi.org/10.3389/ffgc.2022.680262.

Kneeshaw, D.D., Sturtevant, B.R., DeGrandpé, L., Doblas-Miranda, E., James, P.M.A., Tardif, D., Burton, P.J., 2021. The vision of managing for pest-resistant landscapes: realistic or utopic? Current Forestry Reports 7 (2), 97–113. https://doi.org/10.1007/s40725-021-00140-z.

Lague, D., Brodu, N., Leroux, J., 2013. Accurate 3D comparison of complex topography with terrestrial laser scanner: application to the Rangitikei canyon (N-Z). ISPRS J. Photogrammetry Remote Sens. 82, 10–26. https://doi.org/10.1016/j.isprsjprs.2013.04.009.

Lepš, J., Hadincová, V., 1992. How reliable are our vegetation analyses? J. Veg. Sci. 3 (1), 119–124. https://doi.org/10.2307/3236006.

Lloyd, S., 1982. Least squares quantization in PCM. IEEE Trans. Inf. Theor. 28 (2), 129–137. https://doi.org/10.1109/TIT.1982.1056489.

Lucas, C., Bouten, W., Koma, Z., Kissling, W.D., Seijmonsbergen, A.C., 2019. Identification of linear vegetation elements in a rural landscape using LiDAR point clouds. Rem. Sens. 11 (3) https://doi.org/10.3390/rs11030292. Article 3.

Lunetta, R., Congalton, R., Fenstermaker, L., Jensen, J.R., McGwire, K., Tinney, L., 1991. Remote sensing and Geographic Information System data integration: error sources and research issues. Photogramm. Eng. Rem. Sen. 57, 677–687.

Ma, Q., Su, Y., Guo, Q., 2017. Comparison of canopy cover estimations from airborne LiDAR, aerial imagery, and satellite imagery. IEEE J. Sel. Top. Appl. Earth Obs. Rem. Sens. 10 (9), 4225–4236. https://doi.org/10.1109/JSTARS.2017.2711482.

MacLean, D.A., 1984. Effects of spruce budworm outbreaks on the productivity and stability of balsam fir forests. The Forestry Chronicle. https://doi.org/10.5558/tfc60273-5.

MacQueen, J., 1967. Some methods for classification and analysis of multivariate observations. In: Proceedings of the Fifth Berkeley Symposium on Mathematical Statistics and Probability, 1. University of California Press, pp. 281–298. Statistics: Vol. 5.1. https://www.cs.cmu.edu/~bhiksha/courses/mlsp.fall2010/class14/macqueen.pdf.

Mallet, C., Bretar, F., Roux, M., Soergel, U., Heipke, C., 2011. Relevance assessment of full-waveform lidar data for urban area classification. ISPRS J. Photogrammetry Remote Sens. 66 (6), S71–S84. https://doi.org/10.1016/j.isprsjprs.2011.09.008.

Marinelli, D., Coops, N.C., Bolton, D.K., Bruzzone, L., 2018. An unsupervised change detection method for lidar data in forest areas based on change vector analysis in the polar domain. IGARSS 2018 - 2018 IEEE International Geoscience and Remote Sensing Symposium, pp. 1922–1925. https://doi.org/10.1109/IGARSS.2018.8518349.
Mattson, W.J., Simmons, G.A., Witter, J.A., 1988. The spruce budworm in Eastern North America. In: Berryman, A.A. (Ed.), Dynamics of Forest Insect Populations: Patterns, Causes, Implications. Springer US, pp. 309–330. https://doi.org/10.1007/978-1-4899-0789-9_16.
Maynard, D.G., Paré, D., Thiffault, E., Lafleur, B., Hogg, K.E., Kishchuk, B., 2014. How do natural disturbances and human activities affect soils and tree nutrition and growth in the Canadian boreal forest? Environ. Rev. 22 (2), 161–178. https://doi.org/10.1139/er-2013-0057.
Mezey, J.G., Houle, D., 2003. Comparing G matrices: are common principal components informative? Genetics 165 (1), 411–425. https://doi.org/10.1093/genetics/165.1.411.
Milocco, L., Salazar-Ciudad, I., 2022. Evolution of the *G* matrix under nonlinear genotype-phenotype maps. Am. Nat. 199 (3), 420–435. https://doi.org/10.1086/717814.
Ministère des Ressources naturelles et des Forêts, 2023a. Données sur les perturbations naturelles—Insecte: Tordeuse des bourgeons de l'épinette, [Jeu de données], dans Données Québec, 2013, mis à jour le 01 novembre 2023. https://www.donneesquebec.ca/recherche/dataset/donnees-sur-les-perturbations-naturelles-insecte-tordeuse-des-bourgeons-de-lepinette.
Ministère des Ressources naturelles et des Forêts, 2023b. Feux de forêt, [Jeu de données], dans Données Québec, 2017, mis à jour le 18 mars 2024. https://www.donneesquebec.ca/recherche/fr/dataset/feux-de-foret.
Murtagh, F., Contreras, P., 2012. Algorithms for hierarchical clustering: an overview. WIREs Data Mining and Knowledge Discovery 2 (1), 86–97. https://doi.org/10.1002/widm.53.
Nealis, V.G., Régnière, J., 2004. Insect-host relationships influencing disturbance by the spruce budworm in a boreal mixedwood forest. Can. J. For. Res. 34 (9), 1870–1882. https://doi.org/10.1139/x04-061.
Nie, Z., MacLean, D.A., Taylor, A.R., 2018. Forest overstory composition and seedling height influence defoliation of understory regeneration by spruce budworm. For. Ecol. Manag. 409, 353–360. https://doi.org/10.1016/j.foreco.2017.11.033.
Nyström, M., Holmgren, J., Olsson, H., 2012. Prediction of tree biomass in the forest–tundra ecotone using airborne laser scanning. Rem. Sens. Environ. 123, 271–279. https://doi.org/10.1016/j.rse.2012.03.008.
Peng, C., Ma, Z., Lei, X., Zhu, Q., Chen, H., Wang, W., Liu, S., Li, W., Fang, X., Zhou, X., 2011. A drought-induced pervasive increase in tree mortality across Canada's boreal forests. Nat. Clim. Change 1 (9), 467–471. https://doi.org/10.1038/nclimate1293.
Piggott, J.J., Townsend, C.R., Matthaei, C.D., 2015. Reconceptualizing synergism and antagonism among multiple stressors. Ecol. Evol. 5 (7), 1538–1547. https://doi.org/10.1002/ece3.1465.
Régnière, J., Nealis, V.G., 2007. Ecological mechanisms of population change during outbreaks of the spruce budworm. Ecol. Entomol. 32 (5), 461–477. https://doi.org/10.1111/j.1365-2311.2007.00888.x.
Riofrío, J., White, J.C., Tompalski, P., Coops, N.C., Wulder, M.A., 2022. Harmonizing multi-temporal airborne laser scanning point clouds to derive periodic annual height increments in temperate mixedwood forests. Can. J. For. Res. 52 (10), 1334–1352. https://doi.org/10.1139/cjfr-2022-0055.
Robert, L.-E., Sturtevant, B.R., Cooke, B.J., James, P.M.A., Fortin, M.-J., Townsend, P.A., Wolter, P.T., Kneeshaw, D., 2018. Landscape host abundance and configuration regulate periodic outbreak behavior in spruce budworm Choristoneura fumiferana. Ecography 41 (9), 1556–1571. https://doi.org/10.1111/ecog.03553.
Roussel, J.-R., Auty, D., Coops, N.C., Tompalski, P., Goodbody, T.R.H., Meador, A.S., Bourdon, J.-F., de Boissieu, F., Achim, A., 2020. lidR: an R package for analysis of Airborne Laser Scanning (ALS) data. Rem. Sens. Environ. 251, 112061 https://doi.org/10.1016/j.rse.2020.112061.
Roussel, J.-R., Béland, M., Caspersen, J., Achim, A., 2018. A mathematical framework to describe the effect of beam incidence angle on metrics derived from airborne LiDAR: the case of forest canopies approaching turbid medium behaviour. Rem. Sens. Environ. 209, 824–834. https://doi.org/10.1016/j.rse.2017.12.006.
Roussel, J.-R., Caspersen, J., Béland, M., Thomas, S., Achim, A., 2017. Removing bias from LiDAR-based estimates of canopy height: accounting for the effects of pulse density and footprint size. Rem. Sens. Environ. 198, 1–16. https://doi.org/10.1016/j.rse.2017.05.032.
Royama, T., 1984. Population dynamics of the spruce budworm Choristoneura fumiferana. Ecol. Monogr. 54 (4), 429–462. https://doi.org/10.2307/1942595.
Ruel, J.-C., Huot, M., 1993. Impact de la tordeuse des bourgeons de l'épinette [Choristoneura fumiferana (Clem.)] sur la régénération des sapinières après la coupe à blanc. For. Chron. 69 (2), 163–172. https://doi.org/10.5558/tfc69163-2.
Seastedt, T.R., Hobbs, R.J., Suding, K.N., 2008. Management of novel ecosystems: are novel approaches required? Front. Ecol. Environ. 6 (10), 547–553. https://doi.org/10.1890/070046.
Seidl, R., Thom, D., Kautz, M., Martin-Benito, D., Peltoniemi, M., Vacchiano, G., Wild, J., Ascoli, D., Petr, M., Honkaniemi, J., Lexer, M.J., Trotsiuk, V., Mairota, P., Svoboda, M., Fabrika, M., Nagel, T.A., Reyer, C.P.O., 2017. Forest disturbances under climate change. Nat. Clim. Change 7 (6), 395–402. https://doi.org/10.1038/nclimate3303.
Seidler, R., Bawa, K.S., 2001. Logged forests. In: Levin, S.A. (Ed.), Encyclopedia of Biodiversity. Elsevier, pp. 747–760. https://doi.org/10.1016/B0-12-226865-2/00178-4.
Senf, C., Seidl, R., Hostert, P., 2017. Remote sensing of forest insect disturbances: current state and future directions. Int. J. Appl. Earth Obs. Geoinf. 60, 49–60. https://doi.org/10.1016/j.jag.2017.04.004.
Sidak, Z., 1967. Rectangular confidence regions for the means of multivariate normal distributions. J. Am. Stat. Assoc. 62 (318), 626–633. https://doi.org/10.2307/2283989.
Sippel, W.L., 1983. A review of the spruce budworm and its outbreak history. - Federal Open Science Repository of Canada 17–25.
Smith-Tripp, S.M., Coops, N.C., Mulverhill, C., White, J.C., Axelson, J., 2024. Landsat assessment of variable spectral recovery linked to post-fire forest structure in dry sub-boreal forests. ISPRS J. Photogrammetry Remote Sens. 208, 121–135. https://doi.org/10.1016/j.isprsjprs.2024.01.008.
Snelder, T., Lehmann, A., Lamouroux, N., Leathwick, J., Allenbach, K., 2010. Effect of classification procedure on the performance of numerically defined ecological regions. Environ. Manag. 45 (5), 939–952. https://doi.org/10.1007/s00267-010-9465-7.
Steppan, S.J., Phillips, P.C., Houle, D., 2002. Comparative quantitative genetics: evolution of the G matrix. Trends Ecol. Evol. 17 (7), 320–327. https://doi.org/10.1016/S0169-5347(02)02505-3.
Thompson, I.D., Maher, S.C., Rouillard, D.P., Fryxell, J.M., Baker, J.A., 2007. Accuracy of forest inventory mapping: some implications for boreal forest management. For. Ecol. Manag. 252 (1), 208–221. https://doi.org/10.1016/j.foreco.2007.06.033.
Tompalski, P., Coops, N.C., White, J.C., Goodbody, T.R.H., Hennigar, C.R., Wulder, M.A., Socha, J., Woods, M.E., 2021. Estimating changes in forest attributes and enhancing growth projections: a review of existing approaches and future directions using airborne 3D point cloud data. Current Forestry Reports 7 (1), 1–24. https://doi.org/10.1007/s40725-021-00135-w.
Trumbore, S., Brando, P., Hartmann, H., 2015. Forest health and global change. Science 349 (6250), 814–818. https://doi.org/10.1126/science.aac6759.
Turner, M.G., 2010. Disturbance and landscape dynamics in a changing world. Ecology 91 (10), 2833–2849. https://doi.org/10.1890/10-0097.1.
Vastaranta, M., Wulder, M.A., White, J.C., Pekkarinen, A., Tuominen, S., Ginzler, C., Kankare, V., Holopainen, M., Hyyppä, J., Hyyppä, H., 2013. Airborne laser scanning and digital stereo imagery measures of forest structure: comparative results and implications to forest mapping and inventory update. Can. J. Rem. Sens. 39 (5), 382–395. https://doi.org/10.5589/m13-046.
Virgin, G.V.J., MacLean, D.A., 2017. Five decades of balsam fir stand development after spruce budworm-related mortality. For. Ecol. Manag. 400, 129–138. https://doi.org/10.1016/j.foreco.2017.05.057.
Wang, T., Hamann, A., Spittlehouse, D., Carroll, C., 2016. Locally downscaled and spatially customizable climate data for historical and future periods for North America. PLoS One 11 (6), e0156720. https://doi.org/10.1371/journal.pone.0156720.
Ward, J.H., 1963. Hierarchical grouping to optimize an objective function. J. Am. Stat. Assoc. 58 (301), 236–244. https://doi.org/10.2307/2282967.
West, K.F., Webb, B.N., Lersch, J.R., Pothier, S., Triscari, J.M., Iverson, A.E., 2004. Context-driven automated target detection in 3D data. Automatic Target Recognition XIV 5426, 133–143. https://doi.org/10.1117/12.542536.
White, J.C., Coops, N.C., Wulder, M.A., Vastaranta, M., Hilker, T., Tompalski, P., 2016. Remote sensing technologies for enhancing forest inventories: a review. Can. J. Rem. Sens. 42 (5), 619–641. https://doi.org/10.1080/07038992.2016.1207484.
White, J.C., Wulder, M.A., Hermosilla, T., Coops, N.C., Hobart, G.W., 2017. A nationwide annual characterization of 25 years of forest disturbance and recovery for Canada using Landsat time series. Rem. Sens. Environ. 194, 303–321. https://doi.org/10.1016/j.rse.2017.03.035.
White, J.C., Wulder, M.A., Hobart, G.W., Luther, J.E., Hermosilla, T., Griffiths, P., Coops, N.C., Hall, R.J., Hostert, P., Dyk, A., Guindon, L., 2014. Pixel-based image compositing for large-area dense time series applications and science. Can. J. Rem. Sens. 40 (3), 192–212. https://doi.org/10.1080/07038992.2014.945827.
White, J.C., Wulder, M.A., Varhola, A., Vastaranta, M., Coops, N.C., Cook, B.D., Pitt, D., Woods, M., 2013. A best practices guide for generating forest inventory attributes from airborne laser scanning data using an area-based approach. For. Chron. 89 (6), 722–723. https://doi.org/10.5558/tfc2013-132.
Wotherspoon, A., Burnett, M., Bernard, A., Achim, A., Coops, N., 2022. Climate scenarios for Canadian forests. [Technical Report]. . https://doi.org/10.13140/RG.2.2.18449.92009.
Wotherspoon, A.R., Achim, A., Coops, N.C., 2024. Assessing future climate trends and implications for managed forests across Canadian ecozones. Can. J. For. Res. 54 (3), 278–289. https://doi.org/10.1139/cjfr-2023-0058.
Xu, H., Cheng, L., Li, M., Chen, Y., Zhong, L., 2015. Using octrees to detect changes to buildings and trees in the urban environment from airborne LiDAR data. Rem. Sens. 7 (8), 9682–9704. https://doi.org/10.3390/rs70809682.
Zhang, Y., Shen, X., 2013. Direct georeferencing of airborne LiDAR data in national coordinates. ISPRS J. Photogrammetry Remote Sens. 84, 43–51. https://doi.org/10.1016/j.isprsjprs.2013.07.003.